ELSEVIER

NeuroImage

www.elsevier.com/locate/ynimg
NeuroImage xx (2007) xxx–xxx

Time-dependent effects of hyperoxia on the BOLD fMRI signal in primate visual cortex and LGN

Michael Wibral,[a,b,*] Lars Muckli,[a,b] Katharina Melnikovic,[a,b] Bertram Scheller,[c] Arjen Alink,[a,b] Wolf Singer,[a,b] and Matthias H. Munk[a,b]

[a]*Max Planck Institute for Brain Research, Deutschordenstraße 46, 60528 Frankfurt am Main, Germany*
[b]*Brain Imaging Center Frankfurt, Schleusenweg 2-16, 60590 Frankfurt am Main, Germany*
[c]*Department of Anesthesiology, Johann-Wolfgang-Goethe University Frankfurt am Main, Theodor-Stern-Kai 7, 60590 Frankfurt am Main, Germany*

Received 27 October 2005; revised 24 August 2006; accepted 12 December 2006

Hyperoxia is present in many anaesthesia protocols used in animal blood oxygen level-dependent (BOLD) functional magnetic resonance imaging (fMRI) studies. However, little data exist on the influence of hyperoxia on the magnitude of stimulus-induced relative changes in BOLD fMRI signal (ΔBOLD%). No study to date has investigated these effects in a time-resolved manner, although cerebral vasoregulation offers sites for a time-dependent interaction of hyperoxia and ΔBOLD%. Here we investigated time-dependent effects of an inspiratory oxygen fraction of 90%. We tightly clamped end tidal CO_2 and body temperature and recorded physiological parameters relevant to rCBF in (fentanyl/isoflurane) anaesthetized monkeys while using visual stimulation to elicit ΔBOLD%. To clarify whether changes in ΔBOLD% arose from changes in baseline blood oxygenation or rather altered neuronal or vascular reactivity, we directly measured changes in rCBV using monocrystalline ion oxide nanoparticles (MION) as contrast agent. In visual cortex we found a biphasic modulation of stimulus-induced ΔBOLD% under hyperoxia: We observed first a significant decrease in ΔBOLD% by −24% for data averaged over the time interval of 0–180 min post onset of hyperoxia followed by a subsequent recovery to baseline. rCBV response amplitudes were decreased by 21% in the same time interval (0–180 min). In the LGN, we neither found a significant modulation of ΔBOLD% nor of MION response amplitude. The cerebrovascular effects of hyperoxia may, therefore, be regionally specific and cannot be explained by a deoxyhemoglobin dilution model accounting for plasma oxygenation without assuming altered neuronal activity or altered neurovascular coupling.

Keywords: Hyperoxia; BOLD; fMRI; Anaesthetized; Deoxyhemoglobin dilution model

Introduction

Functional magnetic resonance imaging (fMRI) using the blood oxygen level-dependent (BOLD) effect (Ogawa et al., 1990) has become an indispensable tool in human brain mapping due to its non-invasive nature. BOLD fMRI indirectly measures neuronal activity by exploiting the fact that intra voxel field homogeneity in the brain is reduced by the presence of paramagnetic deoxyhemoglobin (dHb) molecules in an imaging voxel. Neuronal activation leads to disproportionate focal increases in regional cerebral blood flow (rCBF). This local hyperperfusion then reduces the total deoxyhemoglobin content of an imaging voxel of brain tissue. The reduction in turn leads to increased signal strength in MRI sequences sensitive to intravoxel field inhomogeneities. The level of the BOLD signal and its relative changes under stimulation, thus, sensitively depend on physiological baseline conditions (Sicard and Duong, 2005) and the gain of neurovascular coupling.

The influence of an augmented oxygen fraction in the breathing gas on baseline CBF has been extensively studied since the first experiments were made more than 50 years ago (Kety and Schmidt, 1948). Multiple studies found the effect of hyperoxia to be a reduction of basal rCBF (Omae et al., 1998; Watson et al., 2000) that was shown to be independent of the typically accompanying hypocapnia (Floyd et al., 2003). This reduction of rCBF has been consistently demonstrated over a wide range of species and physiological states from anesthetized rats (Atochin et al., 2003; Demchenko et al., 2005) to conscious human subjects (Omae et al., 1998; Watson et al., 2000; Floyd et al., 2003).

The influence of this hyperoxia-induced reduction of regional cerebral blood flow (rCBF) on the relative amplitude of stimulus-induced hemodynamic changes has been studied far less extensively, however, and with contradictory results (increase: Kashikura et al., 2000; decrease: Lindauer et al., 2003). Furthermore the effects of hyperoxia seem to depend on time as experiments using very short lasting hyperoxia of 7 min found no effects (Wolf et al., 1997).

Experiments using fMRI under hyperoxic conditions can also yield valuable information on neurovascular coupling mechanisms

* Corresponding author. Brain Imaging Center Frankfurt am Main, Schleusenweg 2 - 16, Haus 95H, 60528 Frankfurt am Main, Germany. Fax: +49 69 630183231.
E-mail address: Wibral@bic.uni-frankfurt.de (M. Wibral).
Available online on ScienceDirect (www.sciencedirect.com).

1053-8119/$ - see front matter © 2006 Elsevier Inc. All rights reserved.
doi:10.1016/j.neuroimage.2006.12.039

as at least three substances that have been implied to play a role in the signalling cascade (for a recent review see: Iadecola, 2004) are also known to be directly influenced by hyperoxia: *S*-nitroso-hemoglobin (SNOHb) (McMahon et al., 2002; Stamler et al., 1997), prostaglandin E_2 (PGE_2) (Mialon and Barthelemy, 1993) and NO (Atochin et al., 2003).

Last but not least detailed knowledge on the effects of prolonged hyperoxia is desirable as several recent experiments on the foundations of BOLD fMRI employed added oxygen in the breathing gas over longer periods of time (Kim et al., 2000; Kolbitsch et al., 2001; Hendrich et al., 2001; Lee et al., 2001; Kalisch et al., 2001; Devor et al., 2005).

The deoxyhemoglobin dilution model (DDM) developed by Hoge et al. (1999a) provides a basis to theoretically predict the effects of changed basal rCBF on the amplitude of stimulus-induced BOLD fMRI signal changes. It has been successfully applied in the case of rCBF changes induced by CO_2 gas challenges. Here the DDM correctly predicted both the increase of relative stimulus-induced signal changes for reduced basal rCBF under hypocapnia and the reduction of relative stimulus-induced signal changes for increased basal rCBF under hypercapnia (Cohen et al., 2002). For the case of severe hyperoxia the classical DDM must fail however, as it assumes a strict proportionality of deoxyhemoglobin (dHb) production and the cerebral metabolic rate of oxygen consumption ($CMRO_2$). This assumption is violated under hyperoxia because non-negligible amounts of oxygen are transported physically dissolved in the blood plasma (approximately 1.8 vol.% at FiO_2 100% (Piantadosi, 1999)). This physically dissolved oxygen is metabolized fully before deoxyhemoglobin 'production' starts as it is closer to the mitochondria on the oxygen pathway. This amount of physically dissolved oxygen has to be directly subtracted from the amount of oxygen taken from oxyhemoglobin under normal physiological conditions (approximately 8 vol.% at normal flow conditions). The dependency between deoxyhemoglobin concentration and $CMRO_2$ is thus changed from a proportional to a merely linear one. In Appendix A, we derive a modified version of the DDM for non-negligible concentrations of plasma oxygen. This model takes into account both plasma oxygenation and flow effects of hyperoxia and predicts an *additional* increase of relative BOLD fMRI response amplitudes for FiO_2 of 100% when compared to the predictions made by the classical DDM for this case. Deviations from this predicted increase would either indicate a direct influence of hyperoxia on neuronal activity or its direct interaction with mechanisms of neurovascular coupling.

To resolve the issue of conflicting results of previous hyperoxia studies, to provide the missing information on the temporal evolution of the effects of hyperoxia and to test the applicability of the modified DDM for the case of hyperoxia we used a visual stimulation paradigm to elicit BOLD fMRI responses in the visual pathway (lateral geniculate nucleus (LGN) and visual cortex) of macaque monkeys and investigated changes in response strength under prolonged hyperoxia of up to 6 h in a time-resolved manner.

Materials and methods

General

This study was conducted in five parts. In the first part (Pilot Experiment) we aimed to find potential linear and time-independent influences of FiO_2 on stimulus-induced ΔBOLD% and to assess the influence of potential confounding factors. In the second part (Time Course Experiment) we tried to keep all anaesthesia related and all physiological parameters as constant as possible while recording the time course of changes in stimulus-induced ΔBOLD% brought about by a single step in FiO_2 from 21% (room air) to 90%. To asses whether changes in vasoreactivity were responsible for the observed effects we then repeated the time course experiment using monocrystalline iron oxide nanoparticles (MION) (Weissleder et al., 1990) as a contrast agent to measure changes in rCBV independent of blood oxygenation (MION Experiment). The fourth part of the study simply consisted in a repetition of the time course experiment in an additional animal (Monkey J) with an experimental schedule that was strongly shifted in time to establish independence of any effects of the circadian rhythm. The fifth part (termed paO_2 Experiment hereafter) was aimed at establishing that arterial hyperoxia is present even at late stages of the experiment. This was necessary as long exposure to an increased inspiratory fraction of oxygen can lead to reduced gas exchange capability of lung tissue and adult respiratory distress syndrome (ARDS) as shown in primates by Huang et al. (1994). Although arterial oxygen tension was still high above normoxic levels after 24 h (~400 mm Hg) in their study, we nevertheless tried to establish that any time-dependent effects were independent of fluctuations in the level of arterial hyperoxia.

Animal preparation and monitoring

The animal experiments were performed according to the German Law for the Protection of Experimental Animals. The procedures also conformed to the regulations issued by the NIH and the Society for Neuroscience.

Initial BOLD fMRI experiments (pilot experiment and time course experiment) were performed on 3 macaque monkeys (Monkeys: K, B, Se; 1 female (K), weight 5.7–9.7 kg). In the retest BOLD fMRI experiment we measured one additional monkey (J, male, 4.2 kg). The MION experiment comprised four monkeys (Monkeys: K, S, M; P, 3 females). In the paO_2 Experiment we measured two monkeys (J and P, 2 male).

Anaesthesia was prepared by administering atropine sulphate (0.5 mg) i.m. Dissociation was induced by an injection of the barbiturate Methohexital i.m. (30–45 mg/kg). This type of anaesthesia induction provides intact breathing reflexes and minimizes the risk of hypoxic accidents before intubation of the animal. Methohexital is one the most short-lived barbiturates available (Harrison and Sear, 2003). Animals were immediately placed between water heating pads and positioned on their back on a custom-made MR-compatible animal bed. After treating the trachea with lidocaine, the animals were intubated and mechanically ventilated by an MRI-compatible ventilator (Datex Ohmeda Aestiva MRI, Datex–Ohmeda Division Instrumentarium Corp., Finland) with a mixture of 0.30% isoflurane in air. A forearm vein was cannulated and mivacurium chloride (5.3–6.9 mg/(kg h)), fentanyl (2.3–4.1 μg/(kg h)), and saline (0.9 vol.% at rates between 0 (only in the pilot experiment) and 18 ml/(kg h)) were infused. This combination of isoflurane and fentanyl is typically used in human surgery; it was first introduced by Logothetis et al. (1999) for monkey fMRI. It is known to provide excellent signal quality. To record vital parameters we used an MRI compatible anaesthesia monitor (Datex Ohmeda S5 MRI) that provided monitoring of the electrocardiogram (ECG), non-invasive monitoring of oxygen

Please cite this article as: Wibral, M., et al., Time-dependent effects of hyperoxia on the BOLD fMRI signal in primate visual cortex and LGN, NeuroImage (2007), doi:10.1016/j.neuroimage.2006.12.039

saturation (SpO_2) via infrared pulse oxymetry, breathing gas analysis (CO_2, O_2, isoflurane) and non-invasive blood pressure (NIBP) measurement. In addition, body temperature was measured via a small Pt100 rectal probe. Body temperature, end tidal CO_2 and isoflurane levels were kept as constant as possible (cf. Table 1) using permanent regulation of heating, isoflurane settings and stroke rate of the ventilator by an operator. We used single-shot EPI imaging that fully samples the breathing cycle and does not suffer from a within-image phase error due to breathing as it is the case for segmented EPI. Thus, we were able to choose a larger stroke volume and low breathing rates (approx. 12 strokes/min) to allow for proper alveolar equilibration of the exhaled breathing gas to ensure correct measurement of end tidal CO_2. To protect the lungs we always used a constant peak end expiratory pressure (PEEP) of 4 cm H_2O.

We chose to use a slightly elevated body temperature (38.5 °C) as our target temperature to compensate decreases in brain metabolism due to isoflurane (Hentschke et al., 2005). In addition, we used a slightly hypocapnic (target $EtCO_2 = 4.0\%$) preparation to partially counterbalance the vasodilatation brought about by isoflurane (Matta et al., 1999). Note that both, elevated body temperature and slight hypocapnia are of course rather crude global attempts to correct for the influences of isoflurane on cerebral circulation and metabolism. They were based on results from preliminary experiments and may fail to yield the desired compensation. To protect the animal from scanner noise we placed silicone earplugs. The pupils were dilated and the ciliary muscles relaxed by administering cyclopentolate to each eye. The non-stimulated left eye was closed and covered using a saline-soaked pad. A contact lens (Wöhlk-Contact-Linsen GmbH, Germany) was placed in the stimulated eye to protect the cornea and to ensure that the focal plane was at the location of visual stimulus presentation. Irrigation of the eyes with either cyclopentolate or saline was repeated after each functional MRI scan to prevent drying of the cornea. To avoid stress induced by the need to urinate the bladder was emptied when necessary by massaging the lower abdomen.

Table 1
Number of runs in the pilot experiment broken down by schedule of FiO_2 changes and level of FiO_2

Pilot experiment: FiO_2 schedule			
FiO_2 level (%)	Sequence: 'rising FiO_2'	Sequence: 'identical FiO_2'	Sequence: 'falling FiO_2'
20	n.a.[a]	7	8
30	6	n.a.[b]	8
50	6	n.a.[b]	4
80	4	n.a.[b]	0
90	10	n.a.[b]	n.a.[c]

For each level of FiO_2 in the pilot experiment this table lists the number of times it was reached while increasing FiO_2 or else decreasing it. n.a. denotes categories not applicable for one of the following reasons: [a]As no hypoxia was used in our experiments the level of 21% FiO_2 could only be reached from an higher or equal FiO_2. [b]Because time constants of FiO_2 effects were not measured in the pilot experiment (but compare results of the time course experiment) we chose to not count repetitions of levels of FiO_2 as identical in this table but rather to attribute them to rising or falling FiO_2 depending on whether the last differing level of FiO_2 was below or above the current level respectively. [c]Due to limits of our gas supply it was impossible to reach FiO_2 of 100%, thus the level of 90% FiO_2 only appeared on the rising slope.

When using FiO_2 of 90% for more than 2 h we used a period of 10 strokes at elevated peak end expiratory pressure (8 cm H_2O) after the end of each run to avoid any risk of atelectasis.

Stimulation

Fig. 1 presents the stimulus paradigm and the stimulation setup. We used a black and white concentric checkerboard with spatial frequency approximately scaling according to cortical magnification and reversing contrast at 8 Hz. Stimulation for one experimental run consisted of one block of 28 s of a blank screen baseline (these data were discarded in later analysis) followed by 23 blocks of 24 s of presentation of the checkerboard and 24 s of blank screen. The position of the foveal field of view on the stimulus screen was estimated by backprojecting the blind spot of the eye via a custom-made reversible ophthalmoscope and subsequent calculation of the foveal position using a visual angle of 14°. The stimulus was centred on this position. Due to limitations of setup geometry and fMRI imaging (susceptibility artefacts induced by the petrous bone) we concentrated on presenting the stimulus optimally in the lower visual field, thus activating the dorsal parts of visual cortex more than the ventral parts. Lateral extension of the stimulus was 22°–27° of visual angle, symmetrically around the fovea; vertical extension was 17°–21° of visual angle predominantly in the lower visual field. As the stimulus was seen through the opening of the standard 18-cm birdcage coil, small parts of the visual field were occluded by the rungs of the coil in some of the sessions. The retinotopically corresponding regions in visual cortex were excluded from further analysis.

Magnetic resonance imaging and fMRI data analysis

All experiments were performed in a 3 T magnet (Magnetom Trio, Siemens Medical Solutions, Erlangen, Germany) equipped with a standard 18-cm birdcage coil. A second-order shim localized on occipital cortex including the upper portion of the superior temporal sulcus was performed. T1 weighted images were acquired with a 3D magnetization prepared rapid gradient echo (MPRAGE) sequence (TE = 3.9 ms, TR = 2250 ms, voxel size = $0.5 \times 0.5 \times 0.5$ mm^3). For fMRI experiments volumes of 20–23 slices (simply referred to as 'volume' in the following) were acquired using single-shot EPI (TR = 2000 ms, TE = 30 ms, matrix size 128×88, FOV = 103×150 mm^2 to 115×168 mm^2 – depending on the size of the monkeys head, resulting pixel size (1.17 mm)^2 to (1.31 mm)^2, slice thickness = 1.9 mm). To achieve the desired echo time we used partial Fourier acquisition (75% of *k*-space covered). To avoid arterial inflow artefacts we chose a flip angle of 70° which is well below the calculated Ernst Angle of 77° for a TR of 2000 ms at 3 T. To account for shortened T2* when using microcrystalline ion oxide nanoparticles as an exogenous contrast agent (MION; Weissleder et al., 1990) we shortened the echo time to 25 ms and had to decrease in-plane resolution to 1.5×1.5 mm^2 in the MION experiment. An experimental run consisted of 540 volumes (540×2000 ms = 1080 s). In a typical experimental session (1 day) monkeys stayed in the scanner for 10 h and 10–14 runs were acquired.

fMRI analysis was performed in BrainVoyagerQX® 1.1.8 (www.brainvoyager.com), using standard pre-processing including slice scan time correction, sub-millimetre motion correction with between run coregistration using sinc interpolation, spatial

Please cite this article as: Wibral, M., et al., Time-dependent effects of hyperoxia on the BOLD fMRI signal in primate visual cortex and LGN, NeuroImage (2007), doi:10.1016/j.neuroimage.2006.12.039

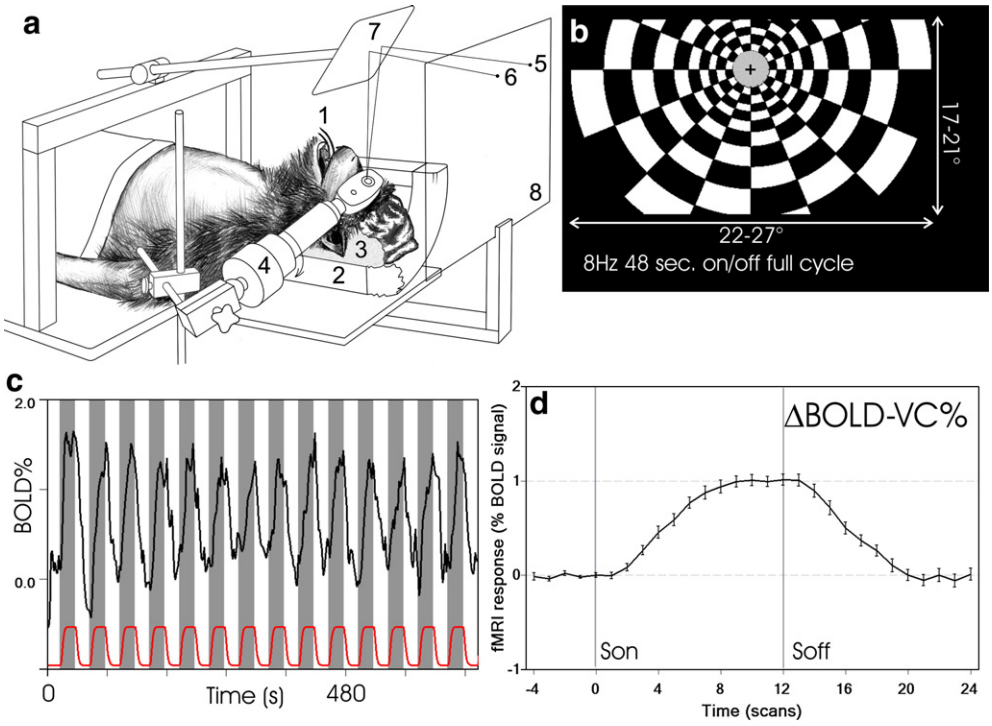

Fig. 1. Stimulation setup and single trial responses. (a) Experimental setup: (1) breathing gas supply: 20% or 90% oxygen, (2) CP birdcage coil (cut, 1/4 shown), (3) vacuum pad, (4) 180° reversible ophthalmoscope, (5) measured position of blind spot, (6) estimated position of fovea at 14° visual angle from blind spot—the stimulus centre is positioned at this location, (7) mirror, (8) back projection screen (b) Schematic drawing of the visual stimulus. The visual angle covered by the stimulus display varied from 22° (horizontal) × 17° (vertical) to 27° × 21° depending on the exact distance between monkey, mirror and stimulation screen. The small cross in the stimulus centre indicates the estimated position of the foveal field of view. Note that we predominantly stimulated the lower visual field to obtain reliable activation in areas without susceptibility artefacts. (c) Single-trial BOLD responses: ΔBOLD% in % of baseline BOLD signal (black) and normalized model hemodynamic response function (red, arbitrary units) versus EPI-volume. Baseline epochs are marked in white, stimulation (23 repetitions) is marked in grey. (d) Single-run average over 23 stimulation epochs. ΔBOLD% in % of baseline BOLD signal versus time counted in EPI volumes (1 TR = 2 s). 'S_{on}' and 'S_{off}' denote onset and offset of the stimulus. Error bars denote ±1 standard error.

smoothing with a 2-mm Gaussian kernel, linear trend removal, temporal high pass at 0.01 Hz and temporal smoothing with 4 s of FWHM (= 2 × TR). fMRI datasets were coregistered to the anatomical image. From the coregistered fMRI slice datasets, volume datasets for 3D analysis were created.

For each experimental session (1 monkey, no removal from scanner) we pooled all functional data and performed a group general linear model (GLM) analysis by using the box car on–off cycles of visual stimulation convolved with a standard hemodynamic response function (Boynton et al., 1996) as a predictor. We then defined regions of interest (ROI) for each experimental session by accepting all voxels that were significant at $p < 0.001$ (Bonferroni corrected for multiple comparison and corrected for serial correlation) if they additionally were part of a cluster of at least 20 voxels.

For each individual run of a session we then extracted time courses averaged separately over all voxels in each of the different ROIs defined by the session GLM with the thresholds given above. Average BOLD signal amplitude for the corresponding two volumes before onset of each single stimulus was defined as the respective baseline for this stimulus repetition. BOLD response amplitudes where calculated relative to this local baseline and subsequently averaged over the 23 stimulus repetitions of a single run to get the amplitude and standard deviation of ΔBOLD% (regionally specific ΔBOLD% is from hereon denoted 'ΔBOLD–VC%' and 'ΔBOLD–LGN%' for visual cortex and the LGN, respectively).

Pilot experiment – influence of anaesthesia parameters and FiO_2

This experiment was designed to investigate the influence of the recorded anaesthesia related covariates and to detect a potential time-independent linear effect of FiO_2 levels on ΔBOLD%. To this end we recorded for each run the initial dose of Methohexital, time elapsed since injection of Methohexital, dose of fentanyl, dose of mivacurium chloride, dose of saline infusion, systolic NIBP, heart rate measured by pulse oxymetry, body temperature at start and end of run, $EtCO_2$ and end tidal fraction of the anaesthetic agent isoflurane (further on abbreviated as FeAA). In addition, we systematically varied FiO_2 of the breathing gas. After a change in FiO_2 we waited for 40 min for the organism to equilibrate before starting the next fMRI acquisition. To further account for longer term hysteresis effects not covered by the 40-min equilibration time we used both possible transitions (i.e. from low to high FiO_2, and from high to low FiO_2) in our design in a balanced manner (Table 1).

Time course experiment

This experiment was designed to investigate the time course of variations in ΔBOLD% in reaction to changes in FiO_2.

Please cite this article as: Wibral, M., et al., Time-dependent effects of hyperoxia on the BOLD fMRI signal in primate visual cortex and LGN, NeuroImage (2007), doi:10.1016/j.neuroimage.2006.12.039

Before acquiring data for this experiment, we monitored BOLD fMRI responses of the monkey in the scanner using the checkerboard stimulus described above and real time data analysis provided by the TurboBrainvoyager® software package (www.brainvoyager.com) in combination with real-time data export from the scanner (Weiskopf et al., 2004, 2005). After waiting for 300 min (two half-lives of the barbiturate Methohexital that was used for anaesthesia induction) we acquired 2–4 fMRI runs at FiO_2 of 21% (room air) followed by a switch to an FiO_2 of 90% and subsequent acquisition of fMRI runs up to a total length of anaesthesia of 720 min (26 runs in total). Alternatively, to investigate the far end of the time course in response to hyperoxia, we switched to an FiO_2 of 90% either immediately after anaesthesia induction or after 300 min had elapsed since induction of anaesthesia (29 runs). In the latter case the switch took place immediately before starting fMRI data acquisition for this experiment. Thus, we were able to record data up to durations of 480 min after switching to hyperoxia, covering the complete time course relevant for fMRI under long term anaesthesia. No single session alone covered the entire duration of hyperoxia presented here, due to the necessary waiting period of 300 min that had to be interposed before obtaining stable data and the length of 480 min under hyperoxia. In sum these times exceeded our chosen limit for continuous anaesthesia (12 h). In addition, to allow for a differentiation of the factors time since anaesthesia induction and time elapsed since switch to hyperoxia, we also performed sessions where FiO_2 was kept constant at 21% (29 runs).

Retest experiment

The aim of this experiment was twofold: First, we wanted to strongly vary the timing of the experiment with respect to the circadian rhythm of the animal to prove independence of any observed effects from this rhythm. Second, we aimed to replicate our experimental results from the time course experiment in an animal that had not been available at that time. Therefore, we measured one additional monkey (J, male) with stimuli and hyperoxia identical to the time course experiment, however, shifting the beginning of the experiment by roughly 7 h with respect to the mean onset of the time course experiments. After an interval of 540 min following the induction of anaesthesia the data acquisition began with two normoxic baseline runs followed by the switch to hyperoxia ($FiO_2 = 90\%$) and acquisition of 8 runs to follow the time course of hyperoxia effects for 270 min. This required continuous anaesthesia for 16 h. Data analysis for this experiment was performed in exactly the same way as for the time course experiment to allow for a later pooling of data from both experiments.

MION experiment

In this experiment we first recorded and analyzed ΔBOLD% in real time as in the preparatory phase of the time course experiment. When a stable signal appeared we recorded the transversal relaxation rate R_2^* (cf. below), and a BOLD fMRI reference run. After this MION was administered IV in a physiological phosphate buffered saline solution at a dose of ~9–11 mg (MION)/kg. We then acquired 2–4 functional EPI runs with MION at FiO_2 of 20% followed by 2–6 runs at FiO_2 of 90%. To account for an elimination of MION from the blood pool (the typical half-life of MION effects (Leite et al., 2002) is comparable with the typical length of our experiments), we first obtained an estimate of R_2^* before and after injecting MION and then after each fMRI run by acquiring single-shot EPI scans using the same slice positions and resolution as in the functional runs but with 6 different echo times (25, 30, 35, 45, 55, and 65 ms).

We extracted the average whole brain signal from several slices and fitted a monoexponential decay function to obtain either $R_{2\ \mathrm{baseline}}^*$ for the runs prior to MION injection or $R_{2\ \mathrm{total}}^*(t) = R_{2\ \mathrm{baseline}}^* + R_{2\ \mathrm{MION}}^*(t)$ after injection of MION.

MION elimination from the blood pool was then modelled by fitting a monoexponential decay function over time to the recorded $R_{2\ \mathrm{MION}}^*(t)$ data to extract the half life of the removal process. This fit was then resampled to get the exact $R_{2\ \mathrm{MION}}^*(t_{\mathrm{midrun}})$ contributed at the middle of an fMRI run.

A ROI was determined for each session by calculating a GLM of all runs with MION using inverted boxcar predictors and thresholding at $p < 0.05$ (Bonferroni corrected for multiple comparison and corrected for serial correlation). We then calculated the average relative response over all voxels inside this ROI and over all repetitions of the stimulus in each given run as in our BOLD fMRI analysis. The response curves obtained for each run were then subjected to global scaling using $R_{2\ \mathrm{MION}}^*(t_{\mathrm{midrun}})$ as described in Leite et al. (2002) and subsequently normalized to the respective baseline values obtained at normoxia in the same session. The globally rescaled and normalized response amplitudes were analysed with respect to the influence of time under hyperoxia. The experiment was repeated in two monkeys.

paO_2 experiment

Animal preparation, hyperoxic ventilation schedule and fMRI data analysis for this experiment were performed identical to the retest experiment. We measured two monkeys (J, P). Under normoxic baseline conditions and under hyperoxic ventilation conditions arterial blood samples were drawn at regular intervals from a catheter placed in the right femoral artery and paO_2 was measured using a blood gas analyzer (Radiometer ABL800 flex, Drott Medizintechnik GmbH, Vienna, Austria). The covered time interval spanned from 414 min before the onset of hyperoxic ventilation to 332 min post onset of hyperoxic ventilation.

Statistical analysis for confound identification

To maximize statistical power for the identification of potentially influential confounds we pooled two datasets: All data from the pilot experiment and those runs from sessions of the time course experiment where FiO_2 was not varied but instead kept at room air level (this combined dataset is further on denoted as 'extended pilot experiment'). These data were then analyzed by linear regression using the inclusion method and the factors: dose of Methohexital, body temperature, $EtCO_2$, time since anaesthesia induction, heart rate, dose of mivacurium chloride, saline infusion rate, FeAA (isoflurane), systolic NIBP, FiO_2 level and a second-order term for the known synergistic interaction between isoflurane and fentanyl (FeAA * fentanyl) (Mcewan et al., 1993).

Statistical analysis of time course data

To ensure maximum protection from the effects of confound variables identified in the pilot experiment we discarded all runs where variations in the values of these confound variables were

Please cite this article as: Wibral, M., et al., Time-dependent effects of hyperoxia on the BOLD fMRI signal in primate visual cortex and LGN, NeuroImage (2007), doi:10.1016/j.neuroimage.2006.12.039

below the 15th percentile or exceeded the 85th percentile of any given confound variable. The resulting rejection limits for extreme values in the confound variables are given in Table 3. Of course, even tighter restrictions would be desirable for improved protection against an influence of confounds. However, even at the current choice of rejection limits the number of data points are in the worst case reduced by a factor of 0.7 per considered confound variable. We, therefore, chose the tightest possible limits that still allowed for a time-resolved post hoc analysis. Data were then subjected to the same multiple linear regression analysis as in the pilot study, this time, however, including the time elapsed since the switch to an FiO_2 of 90% (TIME-O_2-90) and its square (SQTIME-O_2-90) as additional predictors (note that these predictors were not applicable in the pilot experiment). This ensures that any residual influence of confounds does not go undetected while at the same time providing first- and second-order time dependence measures for the effects of hyperoxia. The inclusion of the square of time elapsed since the switch to FiO_2 of 90% (SQTIME-O_2-90) allows the detection of biphasic temporal modulations as they would be brought about for example by two competing pathways of interaction between oxygen and hemodynamic responses.

Finally, to describe the time course of the effects of hyperoxia in detail we performed an ANOVA for a significant influence of the factor time and subsequent post hoc tests (pairwise exact Mann–Whitney *U*) to detect in which time bins BOLD fMRI response amplitudes under hyperoxia varied from their baseline values acquired at normoxic conditions.

Results

Physiological parameters

Table 2 presents an overview of the full range, means and standard deviations of physiological parameters recorded during the total of 148 experimental runs (each comprising 23 stimulus repetitions) in the pilot experiment and the time course experiment. Some extreme values of physiological parameters were not suitable for recording ΔBOLD% and experiments were always immediately stopped upon their occurrence. The recorded means, however, represent a reliable anaesthesia regime for BOLD fMRI in the primate.

Table 2
Descriptive statistics of physiological and anaesthesia parameters across the pilot and the time course experiments

	Mean±S.D.	Range[a] (min–max)	Successfully measured in *n* runs:
Physiological parameters			
Body weight (kg)	7.5±1.6	5.7–9.7	n.a.
NIBP systolic (mm Hg)	120.5±23.5	84–172	128
SpO_2 (%)	99±3	[b]	121
$EtCO_2$ (%)	4.00±0.09	3.75–4.25	148
FeO_2 (%)	52.6±n.a.[c]	21.4–90.3	148
Pulse rate (beats/min)	129±17	84–158	121
Anesthesia parameters			
Methohexital dose (mg/kg)	36.1±4.7	30–45	
Isoflurane level inspiratory (%)	0.30±0.01	0.26–0.32	
Fentanyl (μg/(kg h))	3.0±0.2	2.3–4.1	
Mivacurium chloride (mg/(kg h))	6.3±0.3	5.6–6.9	
Saline 0.5 vol.% (ml/(kg h))	11.1±4.4	1.0–17.4	
Total liquid infusion rate (ml/(kg h))	16.3±4.5	6.0–22.8	

This table gives an overview of recorded physiological and anaesthesia parameters. We list mean, standard deviation and minimum to maximum range of all recorded data (pilot experiment and time course experiment). For some of these variables exceptions apply: [a]Some of the values given as ranges here may indicate a risk to the animal and warrant immediate interruption of the anaesthesia. [b]Deviations in this parameter were due to device malfunction. [c]FiO_2 and hence FeO_2 were systematically varied in both experiments.

BOLD fMRI responses to visual stimulation

In all sessions we were able to obtain regions of interest (ROI) for positive ΔBOLD% at a threshold of $p < 0.001$ (Bonferroni corrected for multiple comparison and corrected for serial correlation) in the lateral geniculate nucleus (LGN, ΔBOLD–LGN%) and the retinotopic visual areas V1/V2/V3 (ΔBOLD–VC %). A typical single-trial BOLD fMRI time course and an averaged response from 23 stimulus repetitions (1 run) from monkey K are presented in Fig. 1. Fig. 2 presents the typical extent of the ROIs in anatomical sections and projected onto the left hemisphere of the reconstructed cortical surface of monkey K.

Extended pilot study – identification of confounds and of FiO_2 level effects

In the extended pilot experiment using a *temporally balanced* schedule of FiO_2 changes we did not observe an influence of the level of FiO_2. The identified confound variables together with their effects sizes are listed in Table 3. Table 3 also lists the resulting limits for influential confound variables that were later used for protecting experimental results of the time course experiment from confounding effects. Note that we found an effect of the time elapsed since the induction of anaesthesia (Fig. 3). Detailed investigation revealed this to be likely an effect of the anaesthetic Methohexital used for induction. The observed process had a half-life between 67 and 138 min (monoexponential fit, simulating the washout of active Methohexital from a biological compartment). We, therefore, chose to limit our data analysis for the subsequent time course experiment to data recorded later than 300 min after induction of anaesthesia. Also note that the identification of influential confounds holds for the particular limits of accuracy in controlling parameters of anaesthesia and physiology in our experiment.

Time course study – time-dependent hyperoxia effects in visual cortex

Fig. 4(b) displays average stimulus-induced BOLD response curves at various times under hyperoxia. The amplitude of BOLD responses was decreased for data averaged over the interval 1–180 min post onset of hyperoxia. Statistical significance of this result was verified using multiple regression analysis (Table 4). Multiple regression analysis revealed that only the time elapsed since switching to FiO_2 of 90% was present as a significant factor in the ΔBOLD–VC% data of the time course experiment. The negative sign of the linear term in time (TIME-O_2-90) and the positive sign of the second-order term (SQTIME-O_2-90) indicate

Please cite this article as: Wibral, M., et al., Time-dependent effects of hyperoxia on the BOLD fMRI signal in primate visual cortex and LGN, NeuroImage (2007), doi:10.1016/j.neuroimage.2006.12.039

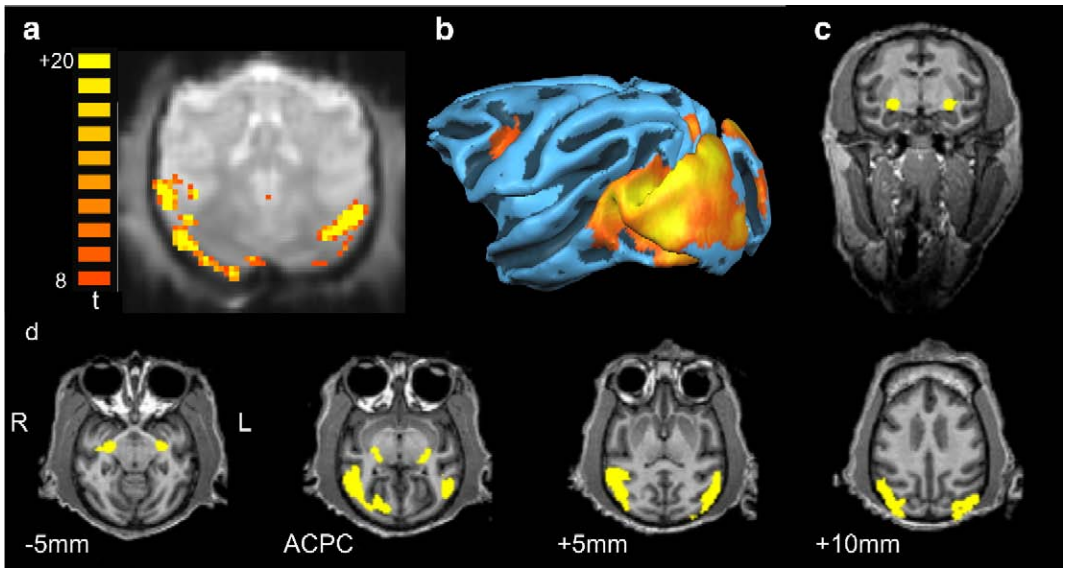

Fig. 2. Localization of ROIs. (a) Single-shot EPI image with overlaid single-run *t*-statistics for activation in visual cortex, thresholded at $t>8$. Colour scale denotes *t* values. (b) Reconstructed cortical grey/white matter boundary with overlaid cortical activation from group GLM analysis comprising data from one session. (c) Localization of ROI in the LGN in a coronal section. (d) Localization of ROIs in visual cortex and LGN on a series of transversal sections on or parallel to the ACPC plane, coordinates indicate distance to ACPC plane (+=dorsal; 'R'=right; 'L'=left). The slight asymmetry of the ROI in visual cortex in this case is most likely due to occlusion of parts of the visual field by rungs of the MRI coil. Note that the upper half of the occipital operculum shows stronger activation (b), an indicator of the predominant stimulation of the lower visual field. However the extent of activated cortex in this case also implies considerable stimulation of the upper visual field.

the presence of a biphasic modulation consisting of an initial drop of ΔBOLD–VC% and a later recovery. The absence of significant effects of confound variables on ΔBOLD–VC% confirms that their influence is successfully controlled by our conservative exclusion limits. It should be noted, however, that a small residual influence of $EtCO_2$ maybe present ($p<0.12$).

To clarify when the drop in ΔBOLD–VC% and the later recovery took place in time we performed a one-way ANOVA with factor TIME-O_2-90 and subsequent post hoc testing. To allow post hoc testing with sufficient data points per time bin we had to choose a rather coarse binning (bin width: 180 min, bins: 'bin 0'=baseline data, 'bin 90'=centred at 90 min of hyperoxia, 'bin 270'=centred at 270 min of hyperoxia). We found a significant influence of factor time ($p<0.007$). Post hoc tests indicated significant differences of bin 0 versus bin 90 (pairwise exact Mann–Whitney *U*, $p<0.002$) and bin 90 versus bin 270 (pairwise exact Mann–Whitney *U*, $p<0.04$), whereas no significant difference was found between bin 0 and bin 270. These results are presented in Fig. 4(d). Please note that while binning was necessary for post hoc testing the existence of time-dependent hyperoxia effects is confirmed independently by the multiple regression analysis. Time course effects are, thus, not an artefact of binning. For exploratory use we also provide a plot of the unrestricted data at a smaller bin width to demonstrate that time-dependent hyperoxia effects are qualitatively similar, independent of bin width (Supplementary Figs. 7c, d).

MION functional rCBV results in visual cortex

The estimated MION half-life varied between 12 min and 243 min (Monkeys K/M/P/S: 12/50/207/243 min). In one of the monkeys

Table 3
Identification of influential confound variables in the extended pilot experiment and the choice of rejection limits for the time course experiment

Identified confound variable (unit)	Coefficient (BOLD%/unit)	Beta[a]	*p*	Lower rejection limit: 15th percentile	Upper rejection limit: 85th percentile
Time since anesthesia induction (min)	0.001	0.53	0.001	n.a.[b] (300)	n.a.[b] (–)
Mean temperature (°C)	0.600	0.39	0.004	38.34	38.60
Fentanyl dose (μg/(kg h))	10.838	5.60	0.025	2.95	3.01
Interaction term: fentanyl FeAA (isoflurane) (μg/(kg h) %)	−36.375	−8.26	0.030	0.79	0.91
Methohexital dose (mg/kg)	0.030	0.41	0.037	30.17	39.33
FeAA (isoflurane) (%)	101.799[c]	5.01	0.040	0.27	0.30

[a] Beta: coefficient values standardized by the variance of the respective predictor observed in our experiments—Beta values should reflect the importance of a confound variable for our data better than the raw coefficients.

[b] Additional analyses indicated that this parameter reflects the washout of the initial anaesthetic Methohexital. We therefore choose to evaluate only data that were recorded later than 300 min after the beginning of anaesthesia.

[c] This large positive coefficient for the level of isofluorane is most likely due to an overestimation of the fentanyl·isofluorane interaction predictor. In fact at a level of ~3 μg fentanyl/(kg h) as it was present in our experiments we get the expected overall negative dependency of ΔBOLD% on isofluorane levels.

Please cite this article as: Wibral, M., et al., Time-dependent effects of hyperoxia on the BOLD fMRI signal in primate visual cortex and LGN, NeuroImage (2007), doi:10.1016/j.neuroimage.2006.12.039

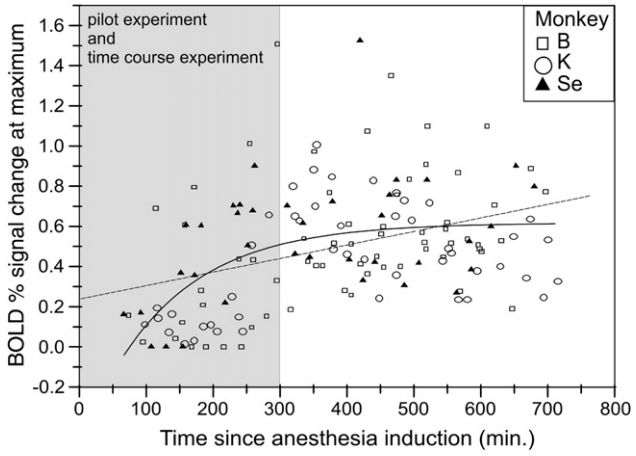

Fig. 3. Effects of Methohexital. BOLD peak amplitudes of the average response curve of single runs (each data point is an average over 23 stimulus repetitions) in visual cortex versus time elapsed since injection of the barbiturate Methohexital in minutes. Data are pooled from the pilot and the time course experiments. Data are given separately for each monkey: open square – monkey B; open circle – monkey K; solid triangle – monkey Se. Dashed line: linear fit of the data, $R^2=0.14$; solid line: exponential relaxation fit of the data: $\Delta\text{BOLD}(t)\% = \Delta\text{BOLD}\%_{max} \times (1-\exp(c \times t))$. The resulting correlation was $R^2=0.23$; the estimated rate constant c is 0.0077 ± 0.0028 min^{-1}. The resulting half-life of the exponential relaxation is between 67 and 138 min. The relaxation fit better describes the data, both quantitatively and qualitatively. Note the saturating character of the development of BOLD amplitudes over time. Also note that data are under the influence of another 9 independent factors, which explains the large amount of variance not accounted for by the fitted models. The grey box indicates the rejection criterion: data acquired before 300 min (~2 half-lives) are considered contaminated by the influence of initial anaesthesia.

(monkey S), injection of MION in phosphate-buffered saline produced a transient rise in blood pressure above 170 mm Hg. This was most likely due to the amount of administered fluid. Data obtained during this period were excluded from analysis. One further run from one monkey (S) had to be excluded due to an $EtCO_2$ above 4.1%. In monkey M one run had to be discarded due to large signal jumps in the time course, most likely due to an instability of the RF chain of the MR scanner and measurements were discontinued after the appearance of this artefact.

Fig. 4(f) presents the results of time-resolved analysis of MION fMRI response amplitudes in visual cortex in response to hyperoxia. Pooled globally scaled and baseline-normalized MION response amplitudes in visual cortex (Fig. 4f) showed a significant decrease (Mann–Whitney U, $p<0.043$) of functional rCBV response in the time bin from 1 to 180 min after the onset of hyperoxia (bin 90, $n=15$) by 23%. This is consistent with the observed drop in response amplitude for ΔBOLD–VC% in the same time interval.

Time course study – time-dependent hyperoxia effects in the LGN

When analyzing BOLD fMRI response amplitude from LGN using the same multiple regression analysis that was used for the analysis of cortical signals we neither found an effect of TIME-O_2-90 nor an effect of SQTIME-O_2-90 (Table 5). ΔBOLD–LGN% was only significantly modulated by small residual influences of $EtCO_2$ and body temperature.

To exclude the possibility that hyperoxia effects in the LGN were missing due to insufficient contrast to noise ratio (CNR) we computed the average ΔBOLD% response curves and the average standard error of the response over stimulus repetitions at each timepoint of BOLD response curves both, for visual cortex and the LGN. The standard errors were then averaged over all timepoints and runs for the visual cortex and the LGN separately. The ratio of average ΔBOLD% and the average standard error for each region then served as a measure for the respective CNR. We obtained only a very small difference in CNR between visual cortex (CNR = 5.45) and the LGN (CNR = 5.40).

MION functional rCBV results in the LGN

Globally scaled and baseline normalized MION response amplitudes, pooled over all four monkeys, did not reveal a significant difference to baseline in the LGN (Fig. 4e). Note that we also did not observe a modulation of the BOLD fMRI signal (ΔBOLD–LGN%) in this structure in this time bin. Responses in the time bin from 1 to 180 min after the onset of hyperoxia (bin 90) did however show a significant increase in variance (Levene's test, $p<0.026$) in the LGN. Findings in the *LGN* using MION fMRI were opposed to our findings in the *visual cortex* using MION fMRI. Thus, we observe a correspondence of relative BOLD fMRI and MION fMRI signals in both LGN (both measures showed no effect) and visual cortex (decrease of both measures). This suggests that the effects observed in our BOLD fMRI experiment were due to a hyperoxia-related modulation of the amplitude of the stimulus-induced vascular lumen changes.

Results of the retest experiment

Results of the retest experiment can be found in Supplementary Fig. 6. In visual cortex (Supplementary Fig. 6a) we found a decrease of the average ΔBOLD%–VC for the interval from 0 to 180 min post onset of hyperoxia ('bin 90' from the time course experiment) by −53% followed by a smaller recovery of the mean for the interval of 180–270 min (*first* half of bin 270 of the time course experiment) to a level of 69% of the pre-hyperoxia baseline signal. Pooling these data with those from the time course experiment revealed a significant influence of both, the linear term in time (TIME-O_2-90, $p<0.002$) with a negative coefficient and the second-order term (SQTIME-O_2-90, $p<0.009$) with a positive coefficient indicating the presence of a biphasic modulation consisting of an initial drop of ΔBOLD–VC% and a later recovery.

In the LGN (Supplementary Fig. 6b) we observed a slow decrease of ΔBOLD–LGN% over time that did not recover until the end of the measurement. When these data were pooled with the data from the time course experiment and analyzed via stepwise regression analysis we did not observe a significant influence of time under hyperoxia on ΔBOLD–LGN%. This analysis of ΔBOLD–LGN%, however, indicated a residual influence of $EtCO_2$ ($p<0.008$) and body temperature ($p<0.01$).

Results of the paO_2 experiment

Fig. 5 presents the results of the paO_2 Experiment. In this experiment paO_2 was monitored in regular intervals to ensure that stable hyperoxia was present at all times of hyperoxic ventilation

Please cite this article as: Wibral, M., et al., Time-dependent effects of hyperoxia on the BOLD fMRI signal in primate visual cortex and LGN, NeuroImage (2007), doi:10.1016/j.neuroimage.2006.12.039

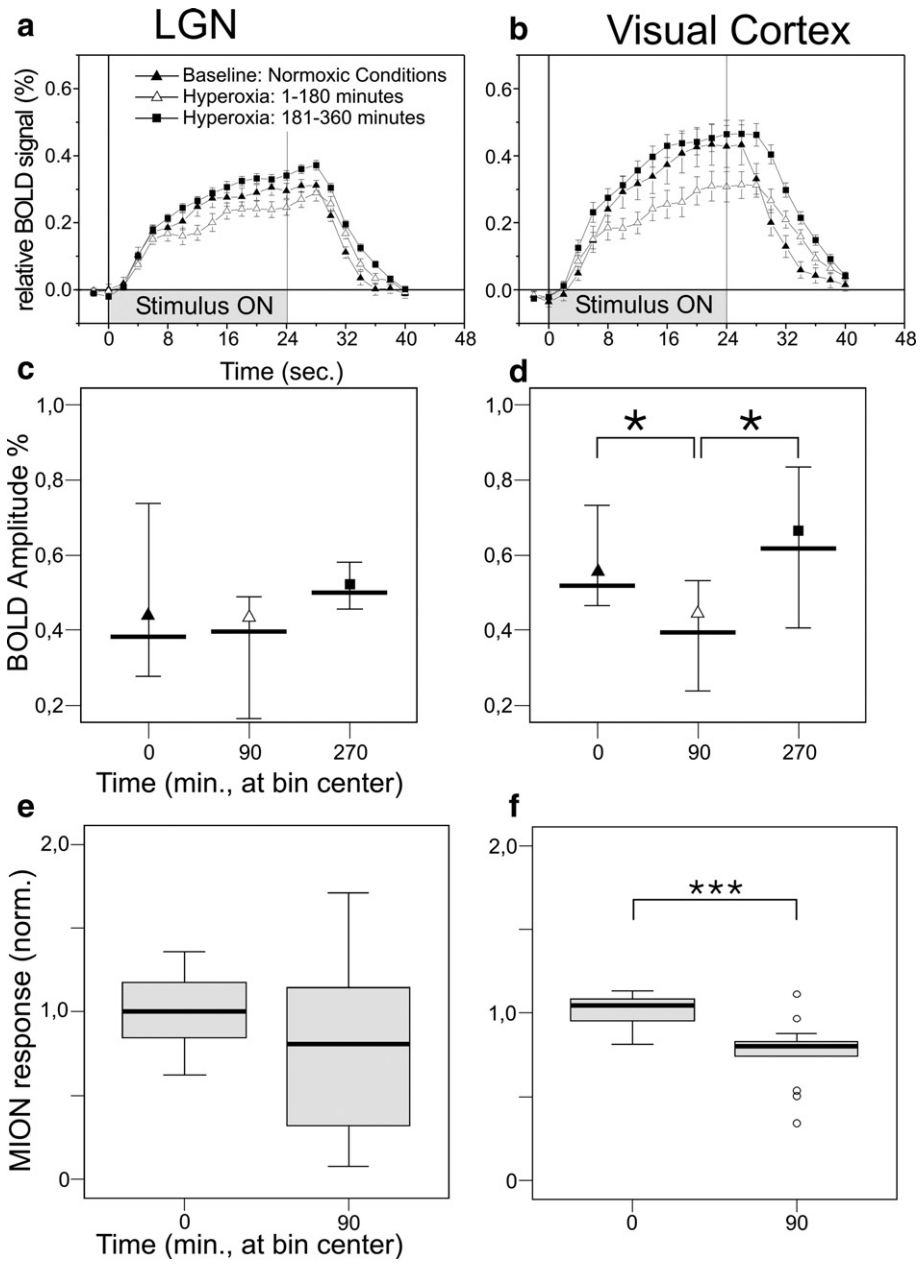

Fig. 4. BOLD fMRI and MION fMRI results for LGN and visual cortex. Left column: a, c, e = results for the LGN. Right column: b, d, e = corresponding results for visual cortex. All error bars indicate the run to run variability, without prior averaging within the separate animals. (a, b) BOLD signal vs. time under stimulation: Average BOLD response curves for different bins of time elapsed under hyperoxic (FiO_2 = 90%) conditions: baseline conditions (normoxia; solid triangle), 1–180 min under hyperoxia (open triangle), 181–360 min under hyperoxia (solid square). Error bars denote one standard error of the mean. All data are recorded later than 300 min after induction of anaesthesia, to avoid effects of the initial anaesthetic Methohexital. Otherwise these curves represent all data acquired in the time course experiment. (c, d) Plot for relative peak BOLD response amplitudes binned over the time intervals given in (a, b) as indicated by the corresponding symbols. The horizontal bars indicate the median values, error bars denote total range in a given bin. Median values for relative peak BOLD response amplitudes in visual cortex are: 0.52 (bin 0); 0.36 (bin 90); 0.62 (bin 270). Bars connect significantly different bins (post hoc, * denotes pairwise exact Mann–Whitney *U*-test, $p < 0.05$). These data are restricted by removal of the 15% lowest and 15% highest values of influential confound variables (cf. Table 3). This restriction was necessary to statistically disambiguate effects of confound variables and of hyperoxia. Numbers of data points in the respective bins of the restricted dataset are: bin 0 = 9 (×23 stimulus rep.), bin 90 = 8 (×23 stimulus rep.), bin 270 = 3 (×23 stimulus rep.). (e, f) MION response amplitudes normalized by baseline response amplitude versus time. Data are pooled in time corresponding to the first two bins in (c, d). ***Asterisks denote statistically significant differences to baseline (Mann–Whitney *U* test, $p < 0.043$). Shaded boxes indicate the 25–75th percentile range. Bars denote the full range of values except statistical outliers. Circles indicate outliers. Number of data points per bin: bin 0, $n = 9$; bin 90, $n = 15$. Note the significant decrease in MION response amplitude for the visual cortex (f) between 1 and 180 min (bin 90) that corresponds to the observed decrease of the BOLD fMRI response amplitudes in visual cortex (b, d).

and that any time-dependent effects observed where not due to fluctuations in the level of paO_2 under hyperoxic ventilation. Results obtained in both monkeys (J, P) for ΔBOLD% in the visual cortex (Fig 5a) and the LGN (Fig. 5b) were qualitatively similar to the statistical results obtained in the time course experiment: ΔBOLD%–VC showed a transient decrease in the time interval

Please cite this article as: Wibral, M., et al., Time-dependent effects of hyperoxia on the BOLD fMRI signal in primate visual cortex and LGN, NeuroImage (2007), doi:10.1016/j.neuroimage.2006.12.039

Table 4
Stepwise linear regression of ΔBOLD% data from the time course experiment—visual cortex

Significant variables (units)	Coefficient (ΔBOLD–VC%/unit)	Beta	p
(Time elapsed since FiO_2 switch)^2 SQTIME-O_2-90 (min^2)	7×10^{-6} [a]	2.36	0.001
Time elapsed since FiO_2 switch TIME-O_2-90 (min)	−0.002 [b]	−1.98	0.004
Excluded variables			
$EtCO_2$			0.104
Time since anesthesia induction			0.176
Heart rate			0.249
Dose of mivacurium chloride			0.343
Saline infusion rate			0.523
FeAA (isoflurane)			0.536
FeAA (isoflurane)·fentanyl			0.557
NIBPsys			0.576
Fentanyl			0.590
Methohexital dose			0.605
Temperature			0.693

[a] The small value of this coefficient is compensated by the large values of the square of the time elapsed since the switch to an FiO_2 of 90%. The significance of this factor is equivalent to a biphasic modulation over time.
[b] The negative sign indicates an initial drop in BOLD response amplitudes.

from 0–180 min post onset of hyperoxic ventilation and ΔBOLD %–LGN remained more stable. Throughout the whole period of hyperoxia a stable arterial hyperoxia was maintained with paO_2 levels high above baseline levels (Fig. 5c; note the vertical axis break). We can therefore exclude the occurrence of hypoxic episodes due to lung injury for the entire duration of the experiment. Furthermore the existing fluctuations in paO_2 under hyperoxic ventilation did not correlate significantly with the observed changes in the BOLD responses in either monkeys (Fig. 5d).

Model predictions

Table 6 presents results for the modulation of ΔBOLD% (given as the ratio $\Delta BOLD\%_{hyperoxia}/\Delta BOLD\%_{normoxia}$) predicted by our modified deoxyhemoglobin dilution model when switching to hyperoxia ($FiO_2 = 90\%$). Results are given for various values of hyperoxia-induced flow reduction ($QCBF := CBF_{hyperoxia}/CBF_{normoxia}$, typical values are between 0.67 and 0.87, refer to Kety and Schmidt (1948) or Floyd et al. (2003)), gain of neurovascular coupling ($n := (\Delta CBF/CBF)/(\Delta CMRO_2/CMRO_2)$) and strength of neuronal activation in terms of increased energy consumption ($\varepsilon = CMRO_{2\ act}/CMRO_{2\ rest}$). Typical values for the increase in neuronal metabolism under visual stimulation can for example be found in (Uludag et al., 2004) and range between 20% and 40%.

The modified DDM (for a derivation see Appendix A) predicts an increase in ΔBOLD% under hyperoxic conditions compared to normoxic conditions for a variety of values of QCBF (0.67; 0.87; (Kety and Schmidt, 1948; Floyd et al., 2003)), ε (1.05, 1.1, 1.2, 1.5) and n (2–6; $n=2$ is the low end of measured values (Hoge et al., 1999b); $n=4$ is derived from a diffusion limited model of oxygen consumption with non-zero mitochondrial O_2 concentration (Buxton, 2002); whereas $n=6$ represents the limit for a diffusion-limited model with zero mitochondrial O_2 concentration and also marks the high end of measured values (Fox and Raichle, 1986)). The predicted modulations of ΔBOLD% (from +19% to +92%) due to hyperoxia are in general higher than those predicted by the classical DDM. Nevertheless even the classical DDM predicted increased ΔBOLD% under hyperoxia, when compared to normoxia (for a derivation of these facts see Appendix A).

Discussion

Hyperoxic ventilation and arterial hyperoxia

Long term exposure to increased levels of oxygen in the inspired breathing gas has effects on several parameters of pulmonary function and can, thus, influence pulmonary gas exchange (for a recent review see Carvalho et al. (1998)). Therefore, ventilation of the animal with increased levels of oxygen does not fully guarantee arterial hyperoxia under all circumstances. Sampling of arterial blood during the measurements provided a control for this source of error. We did not find a systematic decrease of paO_2 over the time interval investigated in the paO_2 experiment and therefore exclude low levels of paO_2 as a cause for the observed time-dependent effects.

Use of a standard hemodynamic response template for model-driven identification of ROIs

Our results demonstrated that hyperoxia changed cerebral hemodynamic responses. In this light the validity of our approach to identify stimulated Regions of Interest (ROI) using a GLM with predictors build from a standard hemodynamic response template may be questioned. At first sight a definition of ROIs based on anatomical landmarks seems like a valid alternative. However, this approach suffers from the fact that the regions of visual cortex in question are not stimulated entirely due to the limits on stimulated visual angles that can be reached with stimulus projection in the scanner bore. Thus, within one anatomical region, activated (stimulated) and inhibited parts of cortex neighbour each other. An

Table 5
Stepwise linear regression of ΔBOLD% data from the time course experiment—lateral geniculate nucleus

Significant variables (units)	Coefficient (ΔBOLD–LGN%/unit)	Beta	p
$EtCO_2$ (%)	−0.754	−0.553	0.008
Mean temperature (°C)	1.860	0.529	0.011
Excluded variables			
(Time elapsed since FiO_2 switch)^2 SQTIME-O_2-90			0.343
Time since anesthesia induction			0.350
Time elapsed since FiO_2 switch TIME-O_2-90			0.405
NIBPsys			0.488
Heart rate			0.507
Methohexital dose			0.587
Saline infusion rate			0.666
FeAA (isoflurane)			0.746
FeAA (isoflurane)·fentanyl			0.752
Fentanyl			0.803
Dose of mivacurium chloride			0.892

Please cite this article as: Wibral, M., et al., Time-dependent effects of hyperoxia on the BOLD fMRI signal in primate visual cortex and LGN, NeuroImage (2007), doi:10.1016/j.neuroimage.2006.12.039

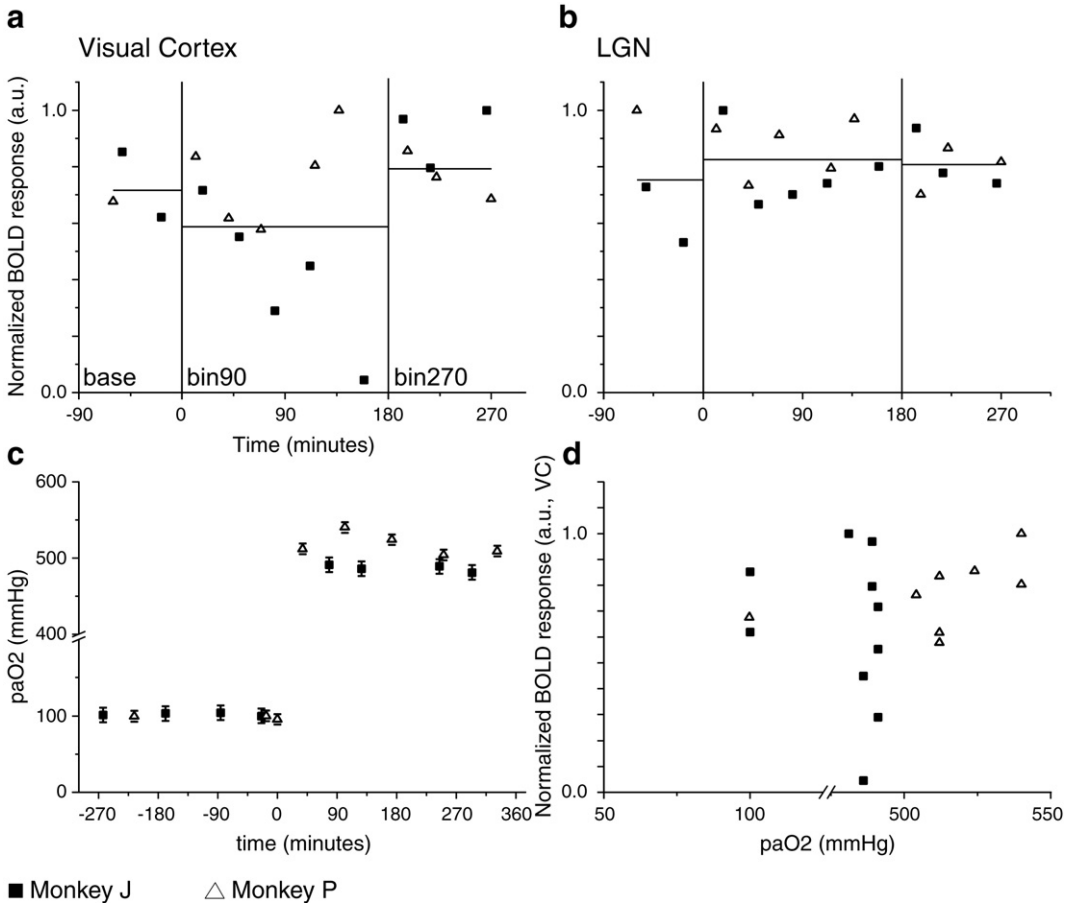

Fig. 5. Time dependence of arterial hyperoxia and BOLD response from the paO_2 Experiment. (a, b) Baseline normalized BOLD signal change over time under hyperoxic ventilation for two monkeys (J, P). Time points before zero denote the normoxic baseline state. Horizontal bars denote bin mean values. (a) Visual cortex, the same biphasic time dependence as in the time course experiment and the retest experiment is found. (b) LGN, no systematic variation of BOLD signal change with respect to time under hyperoxic ventilation is found. (c) Arterial hyperoxia (paO_2) over time under hyperoxic ventilation. Time points before zero denote the normoxic baseline state. Note that a steady state of arterial hyperoxia is maintained throughout the whole period of hyperoxic ventilation (0…360 min). No arterial hypoxia (e.g. due to lung injury) was observed throughout the experiment. (d) Baseline normalized BOLD signal change versus paO_2. The association between the amplitudes observed in a BOLD fMRI run and a corresponding paO_2 value was made by picking the paO_2 value from the blood sampling that was closest in time to the respective BOLD fMRI run. We did not observe a significant correlation between BOLD response levels and fluctuations in the level of paO_2 in either monkey.

anatomical definition of ROIs would, therefore, mix data from entirely different brain processes.

To probe alternative ways of defining ROIs we have, however, used lag correlation analysis of our data with respect to a boxcar function as a model-driven approach with the least possible constraints and in addition we have used the model-free approach of cortex-based spatial ICA (Formisano et al., 2004) on exemplary datasets. In both cases ROIs were largely overlapping with the results of our standard GLM analysis (data not shown).

Influence of confound variables

Results from our pilot experiment indicated that fMRI data recorded in anesthetized animals may be normally dominated by variations in certain confound variables (Table 3). In our experiment we found that a restriction of variations in body temperature in a range of 0.5–1 °C that is usually found in the literature (Wolf et al., 1997; Duong et al., 2001; Lindauer et al., 2003; Sicard and Duong, 2005) was insufficient to measure the effects of hyperoxia without serious confound influence, due to the effect size of the factor body temperature on BOLD response amplitudes (~0.6 ΔBOLD%/°C, pilot experiment, visual cortex; Table 3). Another rather unexpected finding is the long time constant of the effects of the initial anaesthetic Methohexital, which in our study had vascular or neuronal effects influencing ΔBOLD% for up to 5 h, while its direct anaesthetic action is rather short lasting (5–7 min at typical doses used for anaesthesia induction). By discarding data that did not meet our strict criteria on confound variation we could, however, exclude effects of confounds successfully as was demonstrated by the multiple regression analysis. It is worth noting that, for statistical soundness, this procedure requires to identify confound influences from independent data as was done here with data from our pilot study.

Effects of long-term anaesthesia

When an organism is exposed to anaesthesia of considerable length, as in this study, the question about the stability of responses over time inevitably arises independent of the experimental

Please cite this article as: Wibral, M., et al., Time-dependent effects of hyperoxia on the BOLD fMRI signal in primate visual cortex and LGN, NeuroImage (2007), doi:10.1016/j.neuroimage.2006.12.039

Table 6
Model predictions for the ratio $\Delta BOLD\%_{hyperoxia}/\Delta BOLD\%_{normoxia}$ of relative BOLD fMRI signal changes upon stimulation at hyperoxic and normoxic conditions, using a modified deoxyhemoglobin dilution model (DDM) with nonzero plasma oxygen levels

	$\Delta BOLD\%_{hyperoxia}/\Delta BOLD\%_{normoxia}$					
	Gain of neurovascular coupling: *n*					
ε [a]	2	2.5	3	4	5	6
(FiO_2=90%, PDO_2C=1.58 vol.%, QCBF=0.87)						
1.05	1.3871	1.2807	1.2432	1.2125	1.1994	1.1922
1.1	1.4118	1.2949	1.2544	1.2219	1.2081	1.2006
1.2	1.4639	1.3232	1.2765	1.2397	1.2242	1.2158
1.5	1.6470	1.4101	1.3407	1.2883	1.2665	1.2542
(FiO_2=90%, PDO_2C=1.58 vol.%, QCBF=0.67)						
1.05	1.6710	1.5669	1.5303	1.5004	1.4877	1.4807
1.1	1.6953	1.5810	1.5416	1.5099	1.4966	1.4895
1.2	1.7465	1.6091	1.5636	1.5279	1.5132	1.5053
1.5	1.9267	1.6952	1.6276	1.5772	1.5569	1.5459

[a] The parameter ε describes changes in neuronal metabolic demand and is dependent on the stimulation used. Literature values for visual stimulation are typically in the range of 1.2–1.4 (Uludag et al., 2004). To appreciate the effects of the other model parameters, this table should be read at fixed ε values.

manipulation under investigation (hyperoxia). Four measures of precaution were taken in this study to separate effects of hyperoxia from anaesthesia effects:

First, we acquired baseline response data (without hyperoxia) over complete sessions, i.e. even for the very late stages of anaesthesia normoxic data were analyzed. Second, the onset of hyperoxia was jittered with respect to the induction of anaesthesia. Third, time elapsed since anaesthesia induction was kept as a predictor in our multiple regression analysis. This enabled us to detect residual influence of this factor. We did, however, not find a significant contribution. Fourth, in the retest experiment the interval between anaesthesia induction and the onset of hyperoxia was >540 min, introducing yet a bigger jitter than those used in the original hyperoxia experiment to disentangle anaesthesia and hyperoxia effects.

Furthermore it should be noted that the anaesthesia protocol used in this study yielded a rather light anaesthesia. On average animals were fully awake and alert roughly 15 min after ending the administration of anaesthetics. We thus think that the impact of time elapsed under anaesthesia on BOLD fMRI responses did not lead to a systematic error in our results.

Potential effects of BOLD and MION signal baseline changes

When performing fMRI experiments effects of signal baseline drifts might influence results.

We, however, investigated the fractional response amplitudes, relative to an immediately preceding local baseline. While physiological baseline/response effects that are related to the fractional response amplitude are still detectable (and are discussed when trying to explain the failure of the modified deoxyhemoglobin dilution model) simple confounding effects of the physical BOLD signal baseline can be excluded. For our MION experiments measuring the baseline value of T2* (dominating signal intensity) is actually necessary to calibrate the obtained response amplitudes for the amount of MION present in the blood pool. For the MION experiments presented in this article the obtained wash out curves for MION were investigated and no unexpected behaviour was found (data not shown).

Hyperoxia effects – comparison to model predictions

The deoxyhemoglobin dilution model (DDM) as derived by Hoge and colleagues predicts an increase in ΔBOLD% for reduced baseline blood flow as it is encountered for example under hypocapnia. A similar reduced baseline blood flow as in hypocapnia was measured under hyperoxia over a wide range of species and physiological states from anesthetized rats (Demchenko et al., 2005) to conscious human subjects (Floyd et al., 2003). However, the DDM does not apply to this case in a straight forward manner as non negligible concentrations of physically dissolved oxygen in the plasma reduce the proportionality between venous deoxyhemoglobin concentration ($[dHb]_{venous}$) and $CMRO_2$ to a mere linear dependency with an offset. This is because physically dissolved oxygen is metabolized first before significant dissociation of oxygen from haemoglobin can occur. Thus, the equation used by Hoge and colleagues to describe $[dHb]_{venous}$ must be replaced by (for a derivation see Appendix A):

$$[dHb]_{venous} = \frac{CMRO_2 - PDO_2C \cdot CBF}{4 \cdot CBF}$$

Here PDO_2C denotes the concentration of physically dissolved oxygen in the blood plasma. PDO_2C is around 1.5–1.8 vol.% at FiO_2 100% (Piantadosi, 1999). When choosing a PDO_2C of 1.6 vol.% for FiO_2 of 90% our modified DDM (mDDM) predicts a relative increase of ΔBOLD% due to hyperoxia between 19% and 92%, depending on the chosen values for the reduction in CBF under hyperoxia (QCBF), for the increase in neuronal metabolism by stimulation (ε) and the gain of neurovascular coupling (*n*).

Surprisingly our data were in accord neither with the predictions made by the modified deoxyhemoglobin dilution model nor with those made by the classical DDM. We observed no change in ΔBOLD % in the LGN. In visual cortex we observed a *temporary decrease* of ΔBOLD% which was the opposite of our predictions. Responses in visual cortex were first reduced for data averaged from onset of hyperoxia to 180 min, later recordings showed a recovery to pre-hyperoxia baseline amplitudes. Despite this difference between LGN and visual cortex it should be noted that *both* structures failed to show the predicted increases in ΔBOLD%. Thus, measured values in the LGN fall short at least 19% (relative) of the predictions when expressed in units of normoxic ΔBOLD%. Results from visual cortex deviate from the predictions by at least 40%, expressed in the same units. In addition the observed effect in visual cortex was time-dependent, another feature not explained by the modified DDM. Reasons for these deviations may be found in potential violations of one or several assumptions of the modified DDM:

Our derivation of the modified DDM assumed no change in relative stimulation-induced increases of neuronal activity and metabolism under hyperoxia when compared to normoxia. It is known, however, that prolonged high doses of hyperbaric oxygen can produce seizures (Gutsche and Stephen, 1967; for a recent study, see Sato et al., 2001), indicating adaptive changes in the excitability levels of cortical and subcortical networks under hyperoxia. A mechanism of seizure generation based on nNOS-derived NO has recently been proposed by Demchenko and Piantadosi (2006). Changes in nNOS activity may be due to changes in intracellular calcium under hyperoxia as pointed out by Wang et al. (1998). This suggests the

Please cite this article as: Wibral, M., et al., Time-dependent effects of hyperoxia on the BOLD fMRI signal in primate visual cortex and LGN, NeuroImage (2007), doi:10.1016/j.neuroimage.2006.12.039

possibility that weaker effects of hyperoxia on neuronal circuitry exist even at normobaric conditions.

This seemingly conflicts with evidence of unchanged somatosensory evoked potentials under hyperoxia (Lindauer et al., 2003). However, even unchanged evoked potentials do not imply that the total metabolic response to a sensory stimulus is left unchanged under hyperoxia. The non-stimulus-locked parts of the response (often termed 'induced' responses) may contribute significantly to the increased energy consumption after stimulation and correlate well with the BOLD signal (Logothetis et al., 2001) and the very similar response measured with optical recording (Niessing et al., 2005). Therefore, hyperoxia-dependent changes in the induced responses under hyperoxia will strongly alter BOLD fMRI responses but escape a classically evoked potential analysis.

The second assumption in the derivation of the DDM that is probably not met under hyperoxia is that the gain (n) of neurovascular coupling remains constant when switching from normoxic to hyperoxic conditions. It is likely that this gain n changes as a function of direct chemical reactions between increased levels of superoxide radicals under hyperoxia or increased physically dissolved oxygen and substrates involved in neurovascular coupling. Reactions of this kind are known for SNOHb (Stamler et al., 1997; McMahon et al., 2002), PGE_2 (Mialon and Barthelemy, 1993) and NO (Atochin et al., 2003). Further molecules that both play a role in neurovascular coupling and directly interact with excess oxygen may exist. The available data on biological time constants of these reactions and compensatory processes only allow exclusion of certain substances like SNOHb, where time constants of oxygenation effects are on the scale of fractions of a second (McMahon et al., 2002) whereas the effects we observed developed over several tens of minutes. We did not find any data on the time course of basal CBF modulation under normobaric hyperoxia for more than 2 h. Thus, the late recovery we observed could in principle be based on a further reduction of basal CBF and be in accordance with the modified DDM. However, this is rather unlikely as rCBF was reported to rise and not to fall at the later stages of hyperoxia in the hyperbaric case (Atochin et al., 2003).

While one or both of the above-mentioned processes may have contributed to the failure of the modified deoxyhemoglobin dilution model, a potential explanation of our findings must at the same time explain the differences between LGN and visual cortex and the temporal evolution of ΔBOLD% in visual cortex.

We will now discuss the two potential mechanisms of hyperoxic influence that were identified above with respect to their ability to account for all of the observed effects.

Changes in the gain of neurovascular coupling by direct oxygen to modulator/mediator interaction

As outlined above, solid evidence exists for an involvement of NO in the mediation of the effects of hyperoxia on baseline blood flow. A study by Atochin and colleagues on hyperoxia in anesthetized rats which covered exposure durations slightly over an hour (Atochin et al., 2003) provided time-resolved measurements of modulations of basal CBF. Interestingly, in these experiments, a biphasic modulation of basal CBF and of NO availability was observed similar to the biphasic modulation of ΔBOLD% in our experiments. This suggests a possible mechanism for an interaction between hyperoxia and cerebral vasoregulation with two competing pathways having different time constants. Combining this finding of modulated available NO levels over time under hyperoxia with the observation that NO availability modulates hemodynamic response amplitudes (Dirnagl et al., 1993), would account for our findings in visual cortex. This interpretation, however, does not directly explain why we did not find time-dependent effects in the LGN. One possibility is that the changes in the LGN were smaller than in the cortex and hidden in fluctuations caused by other variables. This is supported by the fact that we found residual confound influences for the LGN in the pooled data from time course and retest experiments.

It should be noted that the above-mentioned study by Dirnagl et al. (1993) used systemic or topical application of N^{ω}-nitro-L-arginine (L-NA) which blocks, both, neuronal nitric oxide synthase (nNOS) and endothelial nitric oxide synthase (eNOS). At the vessel this effect is very similar the action of superoxide radicals (present under hyperoxia) that directly react with NO to form the non-vasoactive compound OONO. In their experiment, they measured changes in stimulus-induced rCBF responses only once after 60 min of NO synthase block. Unfortunately, they did not perform time-resolved measurements.

Changes in cortical and thalamic excitability levels

Considering the evidence of hyperoxia-induced epileptic seizures it seems plausible that even small doses of oxygen modulate excitability levels of neuronal networks. Increased neuronal activity due to enhanced excitability is likely to produce increased metabolic demand. This increased background metabolic demand will *decrease*, rather than *increase*, the *fractional* stimulus-driven activity, as reflected by the parameter ε of the model. Ultimately this would yield lower values of ΔBOLD%, as this is also a *relative* measure. Furthermore, a study by Aghakhani et al. (2006) demonstrated the possibility of negative BOLD responses (or, hence, a reduction of response amplitude if added to positive responses) due to epileptic spiking and reported less frequent detection of spiking-related BOLD fMRI responses in the thalamus. This agrees with our observation that hyperoxia effects were only prominent in the cortex. Finally, auto regulatory mechanisms may drive excitability thresholds back to their pre-hyperoxia values—and this could account for the biphasic changes observed in the visual cortex.

In order to further explain the differences between visual cortex and LGN three mechanisms may be considered. First, cortical synapses may exhibit faster and stronger adaptivity under hyperoxia-induced activity changes than thalamic synapses. This is suggested by the fact that changes in the network properties in a deafferentation paradigm lead to rapid reorganization in visual cortex within a few hours (Chino et al., 1992) whereas in the LGN changes were only found after 30 days and later (Eysel et al., 1981). Second, differences may be due to recurrent excitation in the cortex and the lack of such coupling in the LGN. Changes in local excitability are bound to have stronger effects in networks with positive feedback, even though there are inhibitory mechanisms that counteract the build up of supracritical excitation (Douglas et al., 1995). These inhibitory mechanisms may in fact autoregulate excitatory activity after disturbances like the proposed excitability shifts under hyperoxia. Thalamic circuits by contrast are dominated by recurrent inhibitory connections with the corticothalamic projections constituting the only potential feedback loop (Singer et al., 1975).

Third, oxygenation effects on the levels of other neurotransmitters like dopamine (Wang et al., 2003; Adachi et al., 2001) or on GABA transmission (Bickford et al., 1999) may play a role. If modulation of neuronal activity by these transmitters is different between cortex and the LGN (for a recent investigation on the role of dopamine in the

Please cite this article as: Wibral, M., et al., Time-dependent effects of hyperoxia on the BOLD fMRI signal in primate visual cortex and LGN, NeuroImage (2007), doi:10.1016/j.neuroimage.2006.12.039

LGN see Govindaiah and Cox (2006)) the reason for differential effects of hyperoxia may be found here. A layer resolved investigation of the activity in the LGN, which would separate magno- and parvocellular contributions and their corresponding neurotransmitter profiles may shed light on this issue. Unfortunately neither the stimuli used in our study nor the spatial resolution of fMRI as used here can provide such a layer resolved analysis.

While this neuronal model has the potential to account for both, the dissociation of effects between cortex and the LGN and the biphasic time course of the cortical response modulations, more data are required to reach final conclusions:

Data are still lacking on the effect of *normobaric* hyperoxia on neuronal excitability and sustained background activity. Recordings of unit activity and local field potentials under hyperoxia, in combination with fMRI or with optical imaging data (Logothetis et al., 2001; Niessing et al., 2005) could resolve this issue. Data are also missing on the molecular action of excess oxygen and of reactive oxygen species on synaptic transmission. Such effects are likely because superoxide radicals react with neuronally derived NO. Neuronally derived NO serves as second messenger in the adjustment of synaptic transmission (Pape and Mager, 1992).

We would like to emphasize at this point that in the preceding part of the discussion we have been merely assessing the above-mentioned alternatives with respect to their consistency with existing data. As stated above, for a full confirmation of one of the two hypotheses further experiments yielding electrophysiological data are required.

Comparison to existing literature

While not confirming the predictions of our modified DDM, nor of the classical DDM, our results for ΔBOLD–VC% are nevertheless compatible with those of Lindauer and colleagues recorded from rat somatosensory cortex, who observed a decrease in relative stimulus-induced rCBF responses under hyperoxia of 22 min (Lindauer et al., 2003). In contrast to their study and to our results, Kashikura et al. (2000, 2001) measured an increased BOLD fMRI response after the application of hyperoxic conditions for up to 200 s. The difference to our results is likely explained by the fact that Kashikura and colleagues did not stabilize $EtCO_2$. Under hyperoxic conditions $EtCO_2$ and $paCO_2$ are usually altered in freely breathing subjects and animals due to hyperventilation (Floyd et al., 2003; Sicard and Duong, 2005). The reason for this is retention of CO_2 at central chemoreceptors due to reduced binding to haemoglobin under hyperoxia – the Haldane effect (Christiansen et al., 1914; for a review of CO_2 to O_2 interactions in binding to hemoglobin see: Jensen, 2004) – triggering increased breathing rates. Thus, it is possible that the measurements made by Kashikura are dominated by vascular effects of arterial hypocapnia on BOLD fMRI response amplitudes as they were described by Cohen et al. (2002).

Our data, however, are in contradiction to the results of a closely related study by Matsuura et al. (2001). This group investigated relative local cerebral blood flow responses to electrical stimulation of the hind paw in rats both under normoxic and hyperoxic conditions. They found increases in relative response amplitudes at 20–80 min after onset of hyperoxia, while confirming the typical slight vasoconstriction induced by hyperoxia. One potential explanation for the discrepancy observed between the results of Matsuura et al. on one side and those of Lindauer et al. and our results on the other side may lie in the cortical areas investigated. The eyes and the whiskers represent the principal senses for orientation in primates and rats, respectively. This might result in specific adaptivity mechanisms, metabolic demands and vascularisation in these cortices that differ from those of somatosensory cortex responsible for processing of limb sensation. Differences between the modulation of fMRI responses from V1 and somatosensory cortex by hyperoxia have been previously found also by Boakye et al. (2002) under free breathing.

As far as the late effects of prolonged hyperoxia are concerned we are not aware of studies that investigated stimulus-induced hemodynamic responses beyond the time span of 80 min covered in the study of Matsuura et al. (2001).

Our data thus fit the most closely related existing evidence (Lindauer et al., 2003) and extend the knowledge on hyperoxia-induced modulation of functional hemodynamic responses to longer time spans than previously investigated. However, the observed temporary decrease is add odds with the classical theory of the BOLD effect *if* we do *not* assume a direct influence of excess oxygen or superoxide radicals either on neuronal function or the biochemical cascade of neurovascular coupling. Furthermore the observed recovery indicates that at least two competing mechanisms of interaction between oxygen and the BOLD fMRI signal are at work. Although the failure of the classical and the modified DDM may at first seem unsatisfying our new findings may stimulate further research and ultimately foster our understanding of the BOLD effect, especially as the paradigm of excess oxygenation can be easily applied to a large variety of experimental preparations from slices to conscious subjects. Intracortical recordings under hyperoxia show the greatest promise to further our understanding of hyperoxia effects on the brain.

Conclusion

This study presents for the first time a time-resolved analysis of the effects of prolonged normobaric hyperoxia on BOLD fMRI response amplitude. In visual cortex we demonstrated a biphasic behaviour consisting of a transient drop in average BOLD response amplitudes in the time bin from 0 to 180 min after onset of hyperoxia followed by a later recovery to baseline level. Our study supports previous observations made by Lindauer et al. (2003). Functional rCBV response measurements using MION furthermore suggest that these changes were induced by changes in neuronal activity or vasoreactivity under hyperoxia rather than by changes in baseline blood oxygenation. We did not observe any effects in the LGN. Both observations contradict the deoxyhemoglobin dilution model (Hoge et al., 1999a), even though we incorporated the influence of nonzero plasma oxygen levels. The deoxyhemoglobin dilution model and, thus, Davis' formalism for the calculation of $CMRO_2$ (Davis et al., 1998) are, therefore, not applicable to the case of severe hyperoxia. Our results warrant cautious interpretation of studies on functional $CMRO_2$, rCBF and BOLD fMRI signal changes that employ hyperoxia, as the effects of hyperoxia are neither stable over time nor consistent over brain regions.

Acknowledgments

This work received support from the Federal Ministry of Education and Research (Brain Imaging Center Frankfurt, DLR 01GO0203), the German Research Foundation (DFG) and the Max Planck Society. We would like to thank Luc Pellerin and Kamil Uludag for helpful comments on earlier versions of this manuscript. We would also like to thank Johanna Klon-Lipok, Tim Wallenhorst, Nikolaus Weiskopf, Alina Jurcoane, Steffen Volz and Ralf Schoenmeyer for their help with various parts of this experiment.

Please cite this article as: Wibral, M., et al., Time-dependent effects of hyperoxia on the BOLD fMRI signal in primate visual cortex and LGN, NeuroImage (2007), doi:10.1016/j.neuroimage.2006.12.039

Appendix A. Modified deoxyhemoglobin dilution model (mDDM) for non-negligible concentration of oxygen in blood plasma

In their derivation of the DDM, Hoge et al. (1999a) describe the additional transversal relaxation rate $R_2^*|_{\mathrm{dHb}}$ introduced by the presence of deoxyhemoglobin in an imaging voxel by:

$$R_2^*|_{\mathrm{dHb}} = A \cdot \mathrm{CBV} \cdot [\mathrm{dHb}]_{\mathrm{venous}}^{\beta} \tag{1}$$

with A being a sample-specific proportionality constant, $[\mathrm{dHb}]_{\mathrm{venous}}$ the concentration of deoxyhemoglobin in the venous compartment of the voxel and β a constant describing the MR physics of R_2^* signal dephasing (Boxerman et al., 1995). Differences in $[\mathrm{dHb}]_{\mathrm{venous}}$ between the resting state ('rest') and the activated state ('act') after stimulation lead to a difference in $R_2^*|_{\mathrm{dHb}}$ as described by:

$$\Delta R_2^*|_{\mathrm{dHb}} = A \cdot \left(\mathrm{CBV}_{\mathrm{act}} \cdot [\mathrm{dHb}]_{\mathrm{venous,act}}^{\beta} - \mathrm{CBV}_{\mathrm{rest}} \cdot [\mathrm{dHb}]_{\mathrm{venous,rest}}^{\beta} \right) \tag{2}$$

The influence of this difference on the BOLD signal can be written as:

$$\frac{\Delta \mathrm{BOLD}}{\mathrm{BOLD}} = e^{-\mathrm{TE} \cdot \Delta R_2^*|_{\mathrm{dHb}}} - 1 \tag{3}$$

or else, in linear approximation, as:

$$\frac{\Delta \mathrm{BOLD}}{\mathrm{BOLD}} \approx -\mathrm{TE} \cdot \Delta R_2^*|_{\mathrm{dHb}} = \mathrm{TE} \cdot A \cdot \left(\mathrm{CBV}_{\mathrm{rest}} \cdot [\mathrm{dHb}]_{\mathrm{venous,rest}}^{\beta} - \mathrm{CBV}_{\mathrm{act}} \cdot [\mathrm{dHb}]_{\mathrm{venous,act}}^{\beta} \right) \tag{4}$$

Hoge and colleagues, in their derivation, then used the strict proportionality of deoxyhemoglobin concentration to CMRO_2 derived by the conservation of mass principle under normal physiologic conditions:

$$[\mathrm{dHb}]_{\mathrm{venous}} = \frac{1}{4} \frac{\mathrm{CMRO}_2}{\mathrm{CBF}} \tag{5}$$

This equation, however, does not hold under hyperoxic conditions that create a non negligible concentration of physically dissolved oxygen in the plasma (further on abbreviated as $\mathrm{PDO}_2\mathrm{C}$; about 1.8 vol.% at FiO_2 100%, thus providing about 20% of the tissue's oxygen consumption at rest). Because physically dissolved oxygen is metabolized first, the above Eq. (5) has to be rewritten (again using the conservation of mass principle) as:

$$\mathrm{CMRO}_2 = 4 \cdot [\mathrm{dHb}]_{\mathrm{venous}} \cdot \mathrm{CBF} + \mathrm{PDO}_2\mathrm{C} \cdot \mathrm{CBF} \Leftrightarrow [\mathrm{dHb}]_{\mathrm{venous}} = \frac{\mathrm{CMRO}_2 - \mathrm{PDO}_2\mathrm{C} \cdot \mathrm{CBF}}{4 \cdot \mathrm{CBF}} \tag{6}$$

Using Eq. (6) and Grubb's law (Grubb et al., 1974) for the passive relationship of CBV and CBF on the venous side:

$$\frac{\mathrm{CBV}_{\mathrm{act}}}{\mathrm{CBV}_{\mathrm{rest}}} = \left(\frac{\mathrm{CBF}_{\mathrm{act}}}{\mathrm{CBF}_{\mathrm{rest}}} \right)^{\alpha} \tag{7}$$

to replace the various [dHb] and CBV terms in (4) yields:

$$(4) \wedge (6) \wedge (7) \Rightarrow \frac{\Delta \mathrm{BOLD}}{\mathrm{BOLD}} = \mathrm{TE} \cdot A \cdot \mathrm{CBV}_{\mathrm{rest}} \left(\frac{\mathrm{CMRO}_{2\,\mathrm{rest}} - \mathrm{PDO}_2\mathrm{C} \cdot \mathrm{CBF}_{\mathrm{rest}}}{4 \cdot \mathrm{CBF}_{\mathrm{rest}}} \right)^{\beta} \left[1 - \left(\frac{\mathrm{CBF}_{\mathrm{act}}}{\mathrm{CBF}_{\mathrm{rest}}} \right)^{\alpha} \cdot \left(\frac{\frac{\mathrm{CMRO}_{2\,\mathrm{act}} - \mathrm{PDO}_2\mathrm{C} \cdot \mathrm{CBF}_{\mathrm{act}}}{\mathrm{CBF}_{\mathrm{act}}}}{\frac{\mathrm{CMRO}_{2\,\mathrm{rest}} - \mathrm{PDO}_2\mathrm{C} \cdot \mathrm{CBF}_{\mathrm{rest}}}{\mathrm{CBF}_{\mathrm{rest}}}} \right)^{\beta} \right] \tag{8}$$

If we now compare the fractional BOLD response amplitudes ΔBOLD% in the normoxic (n) and hyperoxic (h) state we obtain:

$$\frac{\Delta \mathrm{BOLD}\%_h}{\Delta \mathrm{BOLD}\%_n} = \frac{\frac{\Delta \mathrm{BOLD}_h}{\mathrm{BOLD}_h}}{\frac{\Delta \mathrm{BOLD}_n}{\mathrm{BOLD}_n}} = \ldots$$

$$\frac{\mathrm{CBV}_{h,\mathrm{rest}} \left(\frac{\mathrm{CMRO}_{2\,h,\mathrm{rest}} - \mathrm{PDO}_2\mathrm{C} \cdot \mathrm{CBF}_{h,\mathrm{rest}}}{\mathrm{CBF}_{h,\mathrm{rest}}} \right)^{\beta} \left[1 - \left(\frac{\mathrm{CBF}_{h,\mathrm{act}}}{\mathrm{CBF}_{h,\mathrm{rest}}} \right)^{\alpha} \cdot \left(\frac{\frac{\mathrm{CMRO}_{2\,h,\mathrm{act}} - \mathrm{PDO}_2\mathrm{C} \cdot \mathrm{CBF}_{h,\mathrm{act}}}{\mathrm{CBF}_{h,\mathrm{act}}}}{\frac{\mathrm{CMRO}_{2\,h,\mathrm{rest}} - \mathrm{PDO}_2\mathrm{C} \cdot \mathrm{CBF}_{h,\mathrm{rest}}}{\mathrm{CBF}_{h,\mathrm{rest}}}} \right)^{\beta} \right]}{\mathrm{CBV}_{n,\mathrm{rest}} \left(\frac{\mathrm{CMRO}_{2\,n,\mathrm{rest}}}{\mathrm{CBF}_{n,\mathrm{rest}}} \right)^{\beta} \left[1 - \left(\frac{\mathrm{CBF}_{n,\mathrm{act}}}{\mathrm{CBF}_{n,\mathrm{rest}}} \right)^{\alpha} \cdot \left(\frac{\frac{\mathrm{CMRO}_{2\,n,\mathrm{act}}}{\mathrm{CBF}_{n,\mathrm{act}}}}{\frac{\mathrm{CMRO}_{2\,n,\mathrm{rest}}}{\mathrm{CBF}_{n,\mathrm{rest}}}} \right)^{\beta} \right]} \tag{9}$$

Please cite this article as: Wibral, M., et al., Time-dependent effects of hyperoxia on the BOLD fMRI signal in primate visual cortex and LGN, NeuroImage (2007), doi:10.1016/j.neuroimage.2006.12.039

To simplify this equation we assume equal metabolic rates for the two resting states (hyperoxic (h) and normoxic (n)) and the two activated states (i.e. we assume unchanged neuronal activity under hyperoxia):

$$\mathrm{CMRO_2}_{\,h,\mathrm{act}} = \mathrm{CMRO_2}_{\,n,\mathrm{act}}\,, \quad \mathrm{CMRO_2}_{\,h,\mathrm{rest}} = \mathrm{CMRO_2}_{\,n,\mathrm{rest}} \Rightarrow \frac{\mathrm{CMRO_2}_{\,h,\mathrm{act}}}{\mathrm{CMRO_2}_{\,h,\mathrm{rest}}} = \frac{\mathrm{CMRO_2}_{\,n,\mathrm{act}}}{\mathrm{CMRO_2}_{\,n,\mathrm{rest}}} =: \varepsilon_{\mathrm{neuro}} \tag{10}$$

with $\varepsilon_{\mathrm{neuro}}$ being defined as the relative increase in $\mathrm{CMRO_2}$ upon stimulation. In addition, we use the proportional (multiplicative) model which assumes that changes in blood flow in response to neuronal activation are proportional to the respective resting state CBF for equal changes ε in neuronal activation under conditions n and h:

$$\frac{\mathrm{CBF}_{n,\mathrm{act}}}{\mathrm{CBF}_{n,\mathrm{rest}}} = \frac{\mathrm{CBF}_{h,\mathrm{rest}}}{\mathrm{CBF}_{h,\mathrm{rest}}} =: \delta_{\mathrm{CBF}} \tag{11}$$

Here δ_{CBF} is defined as the factor of increase in CBF that is brought about by *sensory stimulation*.

Furthermore, Grubb's law for the ratio of CBV to CBF now helps to eliminate the remaining CBV terms. Last we rewrite $\mathrm{CMRO_2}_{\,\mathrm{act}}$ in terms of $\mathrm{CMRO_2}_{\,\mathrm{rest}}$ by:

$$\mathrm{CMRO_2}_{\,\mathrm{act}} = \mathrm{CMRO_2}_{\,\mathrm{rest}} \cdot \varepsilon_{\mathrm{neuro}} \tag{12}$$

and then use the fact that this resting state $\mathrm{CMRO_2}$ can be expressed in terms of the oxygen concentration κ (in units of vol.% or, equivalently, ml (O_2)/dl (blood)) that is extracted in the normoxic case at normal flow ($\mathrm{CBF}_{n,\mathrm{rest}}$) and resting conditions:

$$\mathrm{CMRO_2}_{\,\mathrm{rest}} = \kappa \cdot \mathrm{CBF}_{n,\mathrm{rest}} \tag{13}$$

We thus derive:

$$\frac{\frac{\Delta\mathrm{BOLD}_h}{\mathrm{BOLD}_h}}{\frac{\Delta\mathrm{BOLD}_n}{\mathrm{BOLD}_n}} = \ldots \left(\frac{\mathrm{CBF}_{h,\mathrm{rest}}}{\mathrm{CBF}_{n,\mathrm{rest}}}\right)^{\alpha-\beta} \frac{\left(\kappa \cdot \mathrm{CBF}_{n,\mathrm{rest}} - \mathrm{PDO_2C} \cdot \mathrm{CBF}_{h,\mathrm{rest}}\right)^{\beta}\left[1 - \left(\frac{\mathrm{CBF}_{h,\mathrm{act}}}{\mathrm{CBF}_{h,\mathrm{rest}}}\right)^{\alpha} \cdot \left(\frac{\frac{\varepsilon_{\mathrm{neuro}}\kappa \cdot \mathrm{CBF}_{n,\mathrm{rest}} - \mathrm{PDO_2C} \cdot \mathrm{CBF}_{h,\mathrm{rest}} \cdot \delta_{\mathrm{CBF}}}{\mathrm{CBF}_{h,\mathrm{rest}} \cdot \delta_{\mathrm{CBF}}}}{\frac{\kappa \cdot \mathrm{CBF}_{n,\mathrm{rest}} - \mathrm{PDO_2C} \cdot \mathrm{CBF}_{h,\mathrm{rest}}}{\mathrm{CBF}_{h,\mathrm{rest}}}}\right)^{\beta}\right]}{\left(\kappa \cdot \mathrm{CBF}_{n,\mathrm{rest}}\right)^{\beta}\left[1 - \left(\frac{\mathrm{CBF}_{n,\mathrm{act}}}{\mathrm{CBF}_{n,\mathrm{rest}}}\right)^{\alpha} \cdot \left(\frac{\frac{\varepsilon_{\mathrm{neuro}}\kappa \cdot \mathrm{CBF}_{n,\mathrm{rest}}}{\mathrm{CBF}_{n,\mathrm{rest}} \cdot \delta_{\mathrm{CBF}}}}{\frac{\kappa \cdot \mathrm{CBF}_{n,\mathrm{rest}}}{\mathrm{CBF}_{n,\mathrm{rest}}}}\right)^{\beta}\right]} \tag{14}$$

Last, we introduce the quotient of hyperoxic and normoxic resting state blood flow QCBF defined by:

$$\mathrm{QCBF} := \frac{\mathrm{CBF}_{h,\mathrm{rest}}}{\mathrm{CBF}_{n,\mathrm{rest}}} \Leftrightarrow \mathrm{CBF}_{h,\mathrm{rest}} = \mathrm{QCBF} \cdot \mathrm{CBF}_{n,\mathrm{rest}} \tag{15}$$

to obtain:

$$\frac{\frac{\Delta\mathrm{BOLD}_h}{\mathrm{BOLD}_h}}{\frac{\Delta\mathrm{BOLD}_n}{\mathrm{BOLD}_n}} = \left(\mathrm{QCBF}\right)^{\alpha-\beta}\left(\frac{\kappa - \mathrm{PDO_2C} \cdot \mathrm{QCBF}}{\kappa}\right)^{\beta} \frac{\left[1 - \left(\delta_{\mathrm{CBF}}\right)^{\alpha-\beta} \cdot \left(\frac{\varepsilon_{\mathrm{neuro}}\kappa - \mathrm{PDO_2C} \cdot \mathrm{QCBF} \cdot \delta_{\mathrm{CBF}}}{\kappa - \mathrm{PDO_2C} \cdot \mathrm{QCBF}}\right)^{\beta}\right]}{\left[1 - \left(\delta_{\mathrm{CBF}}\right)^{\alpha-\beta} \cdot \left(\varepsilon_{\mathrm{neuro}}\right)^{\beta}\right]} \tag{16}$$

Assuming a fixed coupling of flow to metabolism with gain n:

$$\delta_{\mathrm{CBF}} - 1 = n^*(\varepsilon_{\mathrm{neuro}} - 1) \Leftrightarrow \delta_{\mathrm{CBF}} = n^*(\varepsilon_{\mathrm{neuro}} - 1) + 1 \tag{17}$$

this can be rewritten as:

$$\frac{\frac{\Delta\mathrm{BOLD}_h}{\mathrm{BOLD}_h}}{\frac{\Delta\mathrm{BOLD}_n}{\mathrm{BOLD}_n}} = \left(\mathrm{QCBF}\right)^{\alpha-\beta}\frac{\left(\kappa - \mathrm{PDO_2C} \cdot \mathrm{QCBF}\right)^{\beta}}{\kappa^{\beta}} \cdot \frac{\left[1 - \left(n^*\varepsilon_{\mathrm{neuro}} - n + 1\right)^{\alpha-\beta} \cdot \left(\frac{\varepsilon_{\mathrm{neuro}}\kappa - \mathrm{PDO_2C} \cdot \mathrm{QCBF} \cdot \left(n^*\varepsilon_{\mathrm{neuro}} - n + 1\right)}{8\ \mathrm{vol.\%} - \mathrm{PDO_2C} \cdot \mathrm{QCBF}}\right)^{\beta}\right]}{\left[1 - \left(n^*\varepsilon_{\mathrm{neuro}} - n + 1\right)^{\alpha-\beta} \cdot \left(\varepsilon_{\mathrm{neuro}}\right)^{\beta}\right]} \tag{18}$$

Please cite this article as: Wibral, M., et al., Time-dependent effects of hyperoxia on the BOLD fMRI signal in primate visual cortex and LGN, NeuroImage (2007), doi:10.1016/j.neuroimage.2006.12.039

The first term in Eq. (18) describes the increase of ΔBOLD% by the reduction of baseline flow, the second term changes due to altered baseline deoxyhemoglobin production. The third term describes the effect that an increased flow in the activated state also results in an increased supply of plasma oxygen (per unit time), proportional to flow increase rather than to the increase in metabolism. Numerator and denominator of the third term only differ in the respect that $\varepsilon_{\text{neuro}}{}^{\beta}$ is replaced by:

$$\left(\frac{\varepsilon_{\text{neuro}} 8\ \text{vol.\%} - \text{PDO}_2\text{C}\cdot\text{QCBF}\cdot(n^*\varepsilon_{\text{neuro}} - n + 1)}{8\ \text{vol.\%} - \text{PDO}_2\text{C}\cdot\text{QCBF}}\right)^{\beta} \tag{19}$$

Here corrections made via inclusion of PDO_2C in the denominator are outweighed by those in the numerator when $n,\varepsilon > 1$.

Term 1 (>1) of Eq. (18) is the only contribution found in the classical DDM (with $PDO_2C = 0$ terms 2 and 3 are equal to 1). The contribution of term 3 (>1, response increase) outweighs that of term 2 (<1, response decrease) such that the modified DDM always predicts a greater response amplitude increase under hyperoxia than the classical DDM. This may at first seem counterintuitive as inclusion of a nonzero PDO_2C leads to a decrease of resting state dHb production and, therefore, seemingly raises the baseline at the cost of relative BOLD signal increases. However, under activation conditions a nonzero PDO_2C has the effect of supplying additional oxygen via plasma due to the increased flow. Reduction of [dHb] under activation condition now results from 2 independent mechanisms: dilution by the increased flow and the use of plasma oxygen for a larger fraction of the tissue's increased energy demand. Because the relative increase in flow usually outperforms the increase in metabolism by a factor of 2 or more (for a review see: Uludag, 2005) the fraction of plasma oxygen in total oxygen consumption is effectively increased in the activated state.

We can now derive numerical predictions using:

$$\begin{array}{ll}
\kappa = 8\ \text{vol.\%} & \text{(Piantadosi, 1999)} \\
\text{QCBF} = 0.67;\ 0.87 & \text{(Floyd et al., 2003; Kety and Schmidt, 1948)} \\
\varepsilon_{\text{neuro}} = 1.05 \ldots 1.5 & \text{(assumed } 5-50\% \text{ increase in neuronal metabolism, comp. Uludag, 2004)} \\
\alpha = 0.38 & \text{(Grubb et al., 1974)} \\
\beta = 1.25 & \text{(Boxerman et al., 1995)} \\
\text{PDO}_2\text{C} = 1.5\ \text{vol.\%} & \text{(Piantadosi, 1999)} \\
n = 2 \ldots 6 & \text{(Hoge et al., 1999b; Fox and Raichle, 1986)}
\end{array} \tag{20}$$

Results of these calculations are found in Table 6.

For an exemplary comparison of the classical and the modified DDM we choose $n=2$ and $\varepsilon=1.2$ and obtain:

$$\text{mDDM:}\ \frac{\frac{\Delta\text{BOLD}_h}{\text{BOLD}_h}}{\frac{\Delta\text{BOLD}_n}{\text{BOLD}_n}} = 1.45 \tag{21}$$

compared to:

$$\text{classical DDM:}\ \frac{\frac{\Delta\text{BOLD}_h}{\text{BOLD}_h}}{\frac{\Delta\text{BOLD}_n}{\text{BOLD}_n}} = 1.13. \tag{22}$$

Note last that we are well aware that we omitted the influence of the paramagnetism of O_2 dissolved in the plasma to keep our model simple. The magnetic susceptibility (χ_{O_2}) of pure O_2 at normal conditions (760 mm Hg) is 1.4 ppm. Thus, we expect a contribution of roughly 0.8 ppm for the amounts of physically dissolved O_2 in our experiment at FiO_2 of 90%, if we estimate the O_2 concentration from the measured values presented in (Piantadosi, 1999). In principle signal changes by changed O_2 levels in blood plasma are, therefore, possible. We ignored this contribution to our model of *relative functional signal changes* for the following reason: PDO_2C will be very close to values observed at normoxia after a fraction of the capillary transit time. This is because less than 1/3 of $CMRO_2$ is supplied by this pathway at FiO_2 of 90% and oxygen from the plasma is metabolized first. Direct effects of χ_{O_2} would be, therefore, expected on the arterial side and would, thus, be volume rather than flow effects. Total blood volume changes scale with flow changes to a power of ~0.38 in the steady state (Grubb et al., 1974). Furthermore, there are only very few references describing functional arterial volume changes (e.g., Lee et al., 2001) and in addition the arterial partition of blood volume in a grey matter voxel is around 0.25, thus further limiting a potential direct influence of χ_{O_2}-driven volume effects. Such effects should also have shown up as an *increase* of MION fMRI responses, instead we did observe a decrease of these responses.

Please cite this article as: Wibral, M., et al., Time-dependent effects of hyperoxia on the BOLD fMRI signal in primate visual cortex and LGN, NeuroImage (2007), doi:10.1016/j.neuroimage.2006.12.039

List of abbreviations

Variables		Subscripts	
Name	Description	Name	Description
CBF	Cerebral blood flow	act	Activated state during visual stimulation
CBV	Cerebral blood volume	rest	Resting state, no stimulation
$CMRO_2$	Cerebral metabolic rate of oxygen consumption	h	Hyperoxic conditions
[dHb]	Deoxyhemoglobin concentration	n	Normoxic conditions
α	Grubb's exponent for the passive relationship of CBF and CBV		
β	Constant describing the MR physics of R_2^* signal dephasing (Boxerman et al., 1995)		
δ_{CBF}	Factor of relative increase of CBF under stimulation		
ε	Factor of relative increase of neuronal metabolism under stimulation		
κ	Concentration of oxygen that is extracted at rest an normal flow from deoxyhemoglobin by brain metabolism (in units of ml (O_2)/dl (blood)		
n	Factor describing the proportionality between normalized increases of CBF and $CMRO_2$: $n := (\Delta CBF/CBF)/(\Delta CMRO_2/CMRO_2)$		
ΔBOLD%	Increase in BOLD fMRI signal relative to the (current) baseline		
PDO_2C	Concentration of oxygen dissolved in blood plasma		
QCBF	Ratio of CBF under hyperoxic conditions to CBF at normoxic conditions		

Appendix B. Supplementary data

Supplementary data associated with this article can be found, in the online version, at doi:10.1016/j.neuroimage.2006.12.039.

References

Adachi, Y.U., Watanabe, K., Higuchi, H., Satoh, T., Vizi, E.S., 2001. Oxygen inhalation enhances striatal dopamine metabolism and monoamineoxidase enzyme inhibition prevents it: a microdialysis study. Eur. J. Pharmacol. 422, 61–68.

Aghakhani, Y., Kobayashi, E., Bagshaw, A.P., Hawco, C., Benar, C.G., Dubeau, F., Gotman, J., 2006. Cortical and thalamic fMRI responses in partial epilepsy with focal and bilateral synchronous spikes. Clin. Neurophysiol. 117, 177–191.

Atochin, D.N., Demchenko, I.T., Astern, J., Boso, A.E., Piantadosi, C.A., Huang, P.L., 2003. Contributions of endothelial and neuronal nitric oxide synthases to cerebrovascular responses to hyperoxia. J. Cereb. Blood Flow Metab. 23, 1219–1226.

Bickford, P.C., Chadman, K., Williams, B., Shukitt-Hale, B., Holmes, D., Taglialatela, G., Joseph, J., 1999. Effect of normobaric hyperoxia on two indexes of synaptic function in Fisher 344 rats. Free Radical Biol. Med. 26, 817–824.

Boakye, M., Krauss, B.R., Huckins, S.C., Zhang, L., Szeverenyi, N.M., Hodge Jr., C.J., 2002. Effects of hyperoxia on human sensorimotor cortex activity produced by electrical stimulation of the median nerve: a functional magnetic resonance imaging study. Neurosci. Lett. 321, 5–8.

Boxerman, J.L., Bandettini, P.A., Kwong, K.K., Baker, J.R., Davis, T.L., Rosen, B.R., Weisskoff, R.M., 1995. The intravascular contribution to fMRI signal change: Monte Carlo modeling and diffusion-weighted studies in vivo. Magn. Reson. Med. 34, 4–10.

Boynton, G.M., Engel, S.A., Glover, G.H., Heeger, D.J., 1996. Linear systems analysis of functional magnetic resonance imaging in human V1. J. Neurosci. 16, 4207–4221.

Buxton, R.B., 2002. Coupling between CBF and $CMRO_2$ during neuronal activity. In: Tomita, M., Kanno, I., Hamel, E. (Eds.), Brain Activation and CBF Control. Elsevier Science, The Netherlands, pp. 23–32.

Carvalho, C.R., Paula Pinto, S.G., Maranhao, B., Bethlem, E.P., 1998. Hyperoxia and lung disease. Curr. Opin. Pulm. Med. 4, 300–304.

Chino, Y.M., Kaas, J.H., Smith III, E.L., Langston, A.L., Cheng, H., 1992. Rapid reorganization of cortical maps in adult cats following restricted deafferentation in retina. Vision Res. 32, 789–796.

Christiansen, J., Douglas, C.G., Haldane, J.S., 1914. The absorption and dissociation of carbon dioxide by human blood. J. Physiol. 48, 244–271.

Cohen, E.R., Ugurbil, K., Kim, S.G., 2002. Effect of basal conditions on the magnitude and dynamics of the blood oxygenation level-dependent fMRI response. J. Cereb. Blood Flow Metab. 22, 1042–1053.

Davis, T.L., Kwong, K.K., Weisskoff, R.M., Rosen, B.R., 1998. Calibrated functional MRI: mapping the dynamics of oxidative metabolism. Proc. Natl. Acad. Sci. U. S. A. 95, 1834–1839.

Demchenko, I.T., Piantadosi, C.A., 2006. Nitric oxide amplifies the excitatory to inhibitory neurotransmitter imbalance accelerating oxygen seizures. Undersea Hyperbaric Med. 33, 169–174.

Demchenko, I.T., Luchakov, Y.I., Moskvin, A.N., Gutsaeva, D.R., Allen, B.W., Thalmann, E.D., Piantadosi, C.A., 2005. Cerebral blood flow and brain oxygenation in rats breathing oxygen under pressure. J. Cereb. Blood Flow Metab. 25, 1288–1300.

Devor, A., Ulbert, I., Dunn, A.K., Narayanan, S.N., Jones, S.R., Andermann, M.L., Boas, D.A., Dale, A.M., 2005. Coupling of the cortical hemodynamic response to cortical and thalamic neuronal activity. Proc. Natl. Acad. Sci. U. S. A. 102, 3822–3827.

Dirnagl, U., Lindauer, U., Villringer, A., 1993. Role of nitric oxide in the coupling of cerebral blood flow to neuronal activation in rats. Neurosci. Lett. 149, 43–46.

Douglas, R.J., Koch, C., Mahowald, M., Martin, K.A., Suarez, H.H., 1995. Recurrent excitation in neocortical circuits. Science 269, 981–985.

Duong, T.Q., Iadecola, C., Kim, S.G., 2001. Effect of hyperoxia, hypercapnia, and hypoxia on cerebral interstitial oxygen tension and cerebral blood flow. Magn. Reson. Med. 45, 61–70.

Eysel, U.T., Gonzalez-Aguilar, F., Mayer, U., 1981. Time-dependent decrease in the extent of visual deafferentation in the lateral geniculate nucleus of adult cats with small retinal lesions. Exp. Brain Res. 41, 256–263.

Floyd, T.F., Clark, J.M., Gelfand, R., Detre, J.A., Ratcliffe, S., Guvakov, D., Lambertsen, C.J., Eckenhoff, R.G., 2003. Independent cerebral vasoconstrictive effects of hyperoxia and accompanying arterial hypocapnia at 1 ATA. J. Appl. Physiol. 95, 2453–2461.

Formisano, E., Esposito, F., Di Salle, F., Goebel, R., 2004. Cortex-based independent component analysis of fMRI time series. Magn. Reson. Imaging 22, 1493–1504.

Fox, P.T., Raichle, M.E., 1986. Focal physiological uncoupling of cerebral blood flow and oxidative metabolism during somatosensory stimulation in human subjects. Proc. Natl. Acad. Sci. U. S. A. 83, 1140–1144.

Govindaiah, G., Cox, C.L., 2006. Depression of retinogeniculate synaptic transmission by presynaptic D-2-like dopamine receptors in rat lateral geniculate nucleus. Eur. J. Neurosci. 23, 423–434.

Grubb, R.L., Raichle, M.E., Eichling, J.O., Ter Pogossian, M.M., 1974. The

effects of changes in $PaCO_2$ on cerebral blood volume, blood flow, and vascular mean transit time. Stroke 5, 630–639.

Gutsche, B.B., Stephen, C.R., 1967. Responses of dogs to hyperoxic-, pentylenetetrazol-, and electroshock-induced convulsions. J. Appl. Physiol. 22, 321–326.

Harrison, N.L., Sear, W.S., 2003. Intravenous anaesthetics—Barbiturates, etomidate, propofol, ketamine, and steroids. In: Evers, A.S., Maze, M. (Eds.), Anesthetic Pharmacology: Physiologic Principles and Clinical Practice. Churchill Livingston, Philadelphia, PA, pp. 395–416.

Hendrich, K.S., Kochanek, P.M., Melick, J.A., Schiding, J.K., Statler, K.D., Williams, D.S., Marion, D.W., Ho, C., 2001. Cerebral perfusion during anesthesia with fentanyl, isoflurane, or pentobarbital in normal rats studied by arterial spin-labeled MRI. Magn. Reson. Med. 46, 202–206.

Hentschke, H., Schwarz, C., Antkowiak, B., 2005. Neocortex is the major target of sedative concentrations of volatile anaesthetics: strong depression of firing rates and increase of $GABA_A$ receptor-mediated inhibition. Eur. J. Neurosci. 21, 93–102.

Hoge, R.D., Atkinson, J., Gill, B., Crelier, G.R., Marrett, S., Pike, G.B., 1999a. Investigation of BOLD signal dependence on cerebral blood flow and oxygen consumption: the deoxyhemoglobin dilution model. Magn. Reson. Med. 42, 849–863.

Hoge, R.D., Atkinson, J., Gill, B., Crelier, G.R., Marrett, S., Pike, G.B., 1999b. Linear coupling between cerebral blood flow and oxygen consumption in activated human cortex. Proc. Natl. Acad. Sci. U. S. A. 96, 9403–9408.

Huang, Y.C., Caminiti, S.P., Fawcett, T.A., Moon, R.E., Fracica, P.J., Miller, F.J., Young, S.L., Piantadosi, C.A., 1994. Natural surfactant and hyperoxic lung injury in primates: I. Physiology and biochemistry. J. Appl. Physiol. 76, 991–1001.

Iadecola, C., 2004. Neurovascular regulation in the normal brain and in Alzheimer's disease. Nat. Rev., Neurosci. 5, 347–360.

Jensen, F.B., 2004. Red blood cell pH, the Bohr effect, and other oxygenation-linked phenomena in blood O_2 and CO_2 transport. Acta Physiol. Scand. 182, 215–227.

Kalisch, R., Elbel, G.K., Gossl, C., Czisch, M., Auer, D.P., 2001. Blood pressure changes induced by arterial blood withdrawal influence bold signal in anesthesized rats at 7 Tesla: implications for pharmacologic MRI. NeuroImage 14, 891–898.

Kashikura, K., Kershaw, J., Kashikura, A., Matsuura, T., Kanno, I., 2000. Hyperoxia-enhanced activation-induced hemodynamic response in human VI: an fMRI study. NeuroReport 11, 903–906.

Kashikura, K., Kershaw, J., Kashikura, A., Zhang, X.J., Matsuura, T., Kanno, I., 2001. Hyperoxia modified activation-induced blood oxygenation level-dependent response of human visual cortex (V1): an event-related functional magnetic resonance imaging study. Neurosci. Lett. 299, 53–56.

Kety, S.S., Schmidt, C.F., 1948. The effects of altered arterial tensions of carbon dioxide and oxygen on cerebral blood flow and oxygen consumption of normal young men. J. Clin. Invest. 27, 487–492.

Kim, D.S., Duong, T.Q., Kim, S.G., 2000. High-resolution mapping of iso-orientation columns by fMRI. Nat. Neurosci. 3, 164–169.

Kolbitsch, C., Lorenz, I.H., Hormann, C., Kremser, C., Schocke, M., Felber, S., Moser, P.L., Hinteregger, M., Pfeiffer, K.P., Benzer, A., 2001. Sevoflurane and nitrous oxide increase regional cerebral blood flow (rCBF) and regional cerebral blood volume (rCBV) in a drug-specific manner in human volunteers. Magn. Reson. Imaging 19, 1253–1260.

Lee, S.P., Duong, T.Q., Yang, G., Iadecola, C., Kim, S.G., 2001. Relative changes of cerebral arterial and venous blood volumes during increased cerebral blood flow: implications for BOLD fMRI. Magn. Reson. Med. 45, 791–800.

Leite, F.P., Tsao, D., Vanduffel, W., Fize, D., Sasaki, Y., Wald, L.L., Dale, A.M., Kwong, K.K., Orban, G.A., Rosen, B.R., Tootell, R.B., Mandeville, J.B., 2002. Repeated fMRI using iron oxide contrast agent in awake, behaving macaques at 3 Tesla. NeuroImage 16, 283–294.

Lindauer, U., Gethmann, J., Kuhl, M., Kohl-Bareis, M., Dirnagl, U., 2003. Neuronal activity-induced changes of local cerebral microvascular blood oxygenation in the rat: effect of systemic hyperoxia or hypoxia. Brain Res. 975, 135–140.

Logothetis, N.K., Guggenberger, H., Peled, S., Pauls, J., 1999. Functional imaging of the monkey brain. Nat. Neurosci. 2, 555–562.

Logothetis, N.K., Pauls, J., Augath, M., Trinath, T., Oeltermann, A., 2001. Neurophysiological investigation of the basis of the fMRI signal. Nature 412, 150–157.

Matsuura, T., Kashikura, K., Kanno, I., 2001. Hemodynamics of local cerebral blood flow induced by somatosensory stimulation under normoxia and hyperoxia in rats. Comp. Biochem. Physiol., Part A: Mol. Integr. Physiol. 129, 363–372.

Matta, B.F., Heath, K.J., Tipping, K., Summors, A.C., 1999. Direct cerebral vasodilatory effects of sevoflurane and isoflurane. Anesthesiology 91, 677–680.

Mcewan, A.I., Smith, C., Dyar, O., Goodman, D., Smith, L.R., Glass, P.S., 1993. Isoflurane minimum alveolar concentration reduction by fentanyl. Anesthesiology 78, 864–869.

McMahon, T.J., Moon, R.E., Luschinger, B.P., Carraway, M.S., Stone, A.E., Stolp, B.W., Gow, A.J., Pawloski, J.R., Watke, P., Singel, D.J., Piantadosi, C.A., Stamler, J.S., 2002. Nitric oxide in the human respiratory cycle. Nat. Med. 8, 711–717.

Mialon, P., Barthelemy, L., 1993. Effect of hyperbaric oxygen on prostaglandin and thromboxane synthesis in the cortex and the striatum of rat brain. Mol. Chem. Neuropathol. 20, 181–189.

Niessing, J., Ebisch, B., Schmidt, K.E., Niessing, M., Singer, W., Galuske, R.A., 2005. Hemodynamic signals correlate tightly with synchronized gamma oscillations. Science 309, 948–951.

Ogawa, S., Lee, T.M., Kay, A.R., Tank, D.W., 1990. Brain magnetic resonance imaging with contrast dependent on blood oxygenation. Proc. Natl. Acad. Sci. U. S. A. 87, 9868–9872.

Omae, T., Ibayashi, S., Kusuda, K., Nakamura, H., Yagi, H., Fujishima, M., 1998. Effects of high atmospheric pressure and oxygen on middle cerebral blood flow velocity in humans measured by transcranial Doppler. Stroke 29, 94–97.

Pape, H.C., Mager, R., 1992. Nitric oxide controls oscillatory activity in thalamocortical neurons. Neuron 9, 441–448.

Piantadosi, C.A., 1999. Physiology of hyperbaric hyperoxia. Respir. Care Clin. N. Am. 5, 7–19.

Sato, T., Takeda, Y., Hagioka, S., Zhang, S., Hirakawa, M., 2001. Changes in nitric oxide production and cerebral blood flow before development of hyperbaric oxygen-induced seizures in rats. Brain Res. 918, 131–140.

Sicard, K.M., Duong, T.Q., 2005. Effects of hypoxia, hyperoxia, and hypercapnia on baseline and stimulus-evoked BOLD, CBF, and CMRO (2) in spontaneously breathing animals. NeuroImage 25, 850–858.

Singer, W., Tretter, F., Cynader, M., 1975. Organization of cat striate cortex: a correlation of receptive-field properties with afferent and efferent connections. J. Neurophysiol. 38, 1080–1098.

Stamler, J.S., Jia, L., Eu, J.P., McMahon, T.J., Demchenko, I.T., Bonaventura, J., Gernert, K., Piantadosi, C.A., 1997. Blood flow regulation by *S*-nitrosohemoglobin in the physiological oxygen gradient. Science 276, 2034–2037.

Uludag, K., 2005. Basic principles of functional MRI. In: Edelman, R.R., Hesselink, J.R., Zlatkin, M.B., Crues, J.V. (Eds.), Clinical Magnetic Resonance Imaging. Saunders (W.B.) Co Ltd.

Uludag, K., Dubowitz, D.J., Yoder, E.J., Restom, K., Liu, T.T., Buxton, R.B., 2004. Coupling of cerebral blood flow and oxygen consumption during physiological activation and deactivation measured with fMRI. NeuroImage 23, 148–155.

Wang, W.J., Ho, X.P., Yan, Y.L., Yan, T.H., Li, C.L., 1998. Intrasynaptosomal free calcium and nitric oxide metabolism in central nervous system oxygen toxicity. Aviat. Space Environ. Med. 69, 551–555.

Wang, L., Osborne, P.G., Yu, X., Shangguan, D., Zhao, R., Han, H.W., Liu, G.Q., 2003. Hyperoxia caused by microdialysis perfusion decreased striatal monoamines: involvement of oxidative stress. Neurochem. Int. 42, 465–470.

Watson, N.A., Beards, S.C., Altaf, N., Kassner, A., Jackson, A., 2000. The

Please cite this article as: Wibral, M., et al., Time-dependent effects of hyperoxia on the BOLD fMRI signal in primate visual cortex and LGN, NeuroImage (2007), doi:10.1016/j.neuroimage.2006.12.039

effect of hyperoxia on cerebral blood flow: a study in healthy volunteers using magnetic resonance phase-contrast angiography. Eur. J. Anaesthesiol. 17, 152–159.

Weiskopf, N., Mathiak, K., Bock, S.W., Scharnowski, F., Veit, R., Grodd, W., Goebel, R., Birbaumer, N., 2004. Principles of a brain–computer interface (BCI) based on real-time functional magnetic resonance imaging (fMRI). IEEE Trans. Biomed. Eng. 51, 966–970.

Weiskopf, N., Klose, U., Birbaumer, N., Mathiak, K., 2005. Single-shot compensation of image distortions and BOLD contrast optimization using multi-echo EPI for real-time fMRI. NeuroImage 24, 1068–1079.

Weissleder, R., Elizondo, G., Wittenberg, J., Rabito, C.A., Bengele, H.H., Josephson, L., 1990. Ultrasmall superparamagnetic iron-oxide-characterization of a new class of contrast agents for MR imaging. Radiology 175, 489–493.

Wolf, T., Lindauer, U., Villringer, A., Dirnagl, U., 1997. Excessive oxygen or glucose supply does not alter the blood flow response to somatosensory stimulation or spreading depression in rats. Brain Res. 761, 290–299.

Please cite this article as: Wibral, M., et al., Time-dependent effects of hyperoxia on the BOLD fMRI signal in primate visual cortex and LGN, NeuroImage (2007), doi:10.1016/j.neuroimage.2006.12.039